EGG-TMI-7222
cy-1

EGG-TMI-7222
June 1986

INFORMAL REPORT

ASSESSMENT OF DAMAGE POTENTIAL TO THE TMI-2 LOWER HEAD DUE TO THERMAL ATTACK BY CORE DEBRIS

August W. Cronenberg
Stephen R. Behling
James M. Broughton

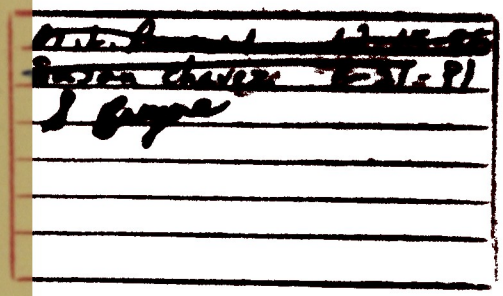

Idaho National Engineering Laboratory

Managed by the U.S. Department of Energy

EG&G Idaho

Work performed under DOE Contract No. DE-AC07-76ID01570

EGG-TMI-7222

ASSESSMENT OF DAMAGE POTENTIAL TO THE TMI-2 LOWER HEAD DUE TO THERMAL ATTACK BY CORE DEBRIS

August W. Cronenberg[a]
Stephen R. Behling
James M. Broughton

Published June 1986

EG&G Idaho, Inc.
Idaho Falls, Idaho 83401

Prepared for the
U.S. Department of Energy
Idaho Operations Office
Under DOE Contract No. DE-AC07-76ID01570

---

a. ESA, Inc., 836 ClairView Lane, Idaho Falls, ID 83402

ABSTRACT

Camera inspection of the Three Mile Island Unit 2 (TMI-2) inlet plenum region has shown that approximately 10 to 20 percent of the core material loading may have relocated to the lower plenum. Although vessel integrity was maintained, a question of primary concern is "how close to vessel failure" did this accident come. This report summarizes the results of thermal analyses aimed at assessing damage potential to the TMI-2 lower head and attached instrument penetration tubes due to thermal attack by hot core debris. Results indicate that the instrument penetration nozzles could have experienced melt failure at localized hot spot regions, with attendant debris drainage and plugging of the instrument lead tubes. However, only minor direct thermal attack of the vessel liner is predicted.

CONTENTS

FIGURES

TABLES

ASSESSMENT OF DAMAGE POTENTIAL TO THE TMI-2 LOWER HEAD DUE TO THERMAL ATTACK BY CORE DEBRIS

INTRODUCTION

Recent camera inspection of the Three Mile Island Unit 2 (TMI-2) lower plenum has shown that approximately 10 to 20% of the core loading may have relocated to the lower plenum. This core relocation was not originally thought to have occurred during the accident. Hence, these findings heighten the issues of debris coolability, melt progression, and potential for bottom head failure of the reactor vessel due to thermal attack by hot core debris. Specifically, unresolved questions remain as to how initial core degradation (i.e., rod ballooning, zircaloy and control rod melting, fuel liquefaction, reflood-induced rod fragmentation, etc.) led to extensive debris migration, the sequence of events leading to such migration, and the consequences and implications of core debris interaction with the lower head. It is important to note at the outset that, although TMI-2 vessel integrity was maintained, the question arises as to whether or not vessel failure could have occurred under somewhat different conditions. This report summarizes results of analysis aimed at assessing thermal damage potential to the TMI-2 lower head forging and the attached instrument penetration tubes.

To interpret the consequences of thermal interaction of core debris with the lower head structure, a brief description is first presented of a plausible sequence of events which may have led to massive migration of core material into the lower plenum. This is followed by a summary of what is currently known of debris characteristics and observations of debris interaction with the lower plenum. Analyses are then presented concerning debris-plenum interaction, and conclusions are drawn relative to the question of the potential for loss of pressure vessel integrity.

ACCIDENT SEQUENCE LEADING TO DEBRIS MIGRATION TO LOWER PLENUM

Various investigators have attempted to reconstruct the TMI-2 accident sequence and resultant core damage scenario.[1-5] What is of particular interest here is the sequence of events which resulted in core debris relocation to the lower plenum and attendant potential for debris thermal attack on the lower head structure.

Analysis indicates that core uncovery started about 100 min after reactor scram, due to loss of feedwater supply to the steam generator and primary system loss of coolant through the pressurizer relief valve. By about 170 min, the core is predicted to have heated to temperatures sufficiently high that the fuel rods ballooned and ruptured; and most of the uncovered portion of the control rods melted. The upper 40 to 60% of the unoxided fuel rod cladding also melted, with attendant attack on and partial dissolution of fuel at a eutectic α-$Zr(O)/UO_2$ melt temperature of 2170 K. This liquefied material is predicted by the SCDAP code[6] to have slumped or drained to the colder bottom region of the core, where coherent blockage formed via freezing, as depicted in Figure 1a.

Upon a temporary restart of primary coolant pump 2B at 174 min, flow diversion around the blockage region is postulated. The oxidized upper regions of the core are predicted to have experienced quench-induced fuel shattering/fragmentation, forming a loose bed of rubble ~0.8 m thick, as shown in Figure 1b. The upper large void was apparently formed by downward movement of material. Only the outside of the coherent blockage region was probably cooled, the inside remaining relatively hot due to continued decay heating by retained fission products. As the water level dropped following the termination of coolant supply, the blockage would experience heatup, due to the combined effects of limited porosity for coolant ingress, low conductivity, large mass, and internal heat generation, resulting in central blockage temperatures exceeding the melting point.[5]

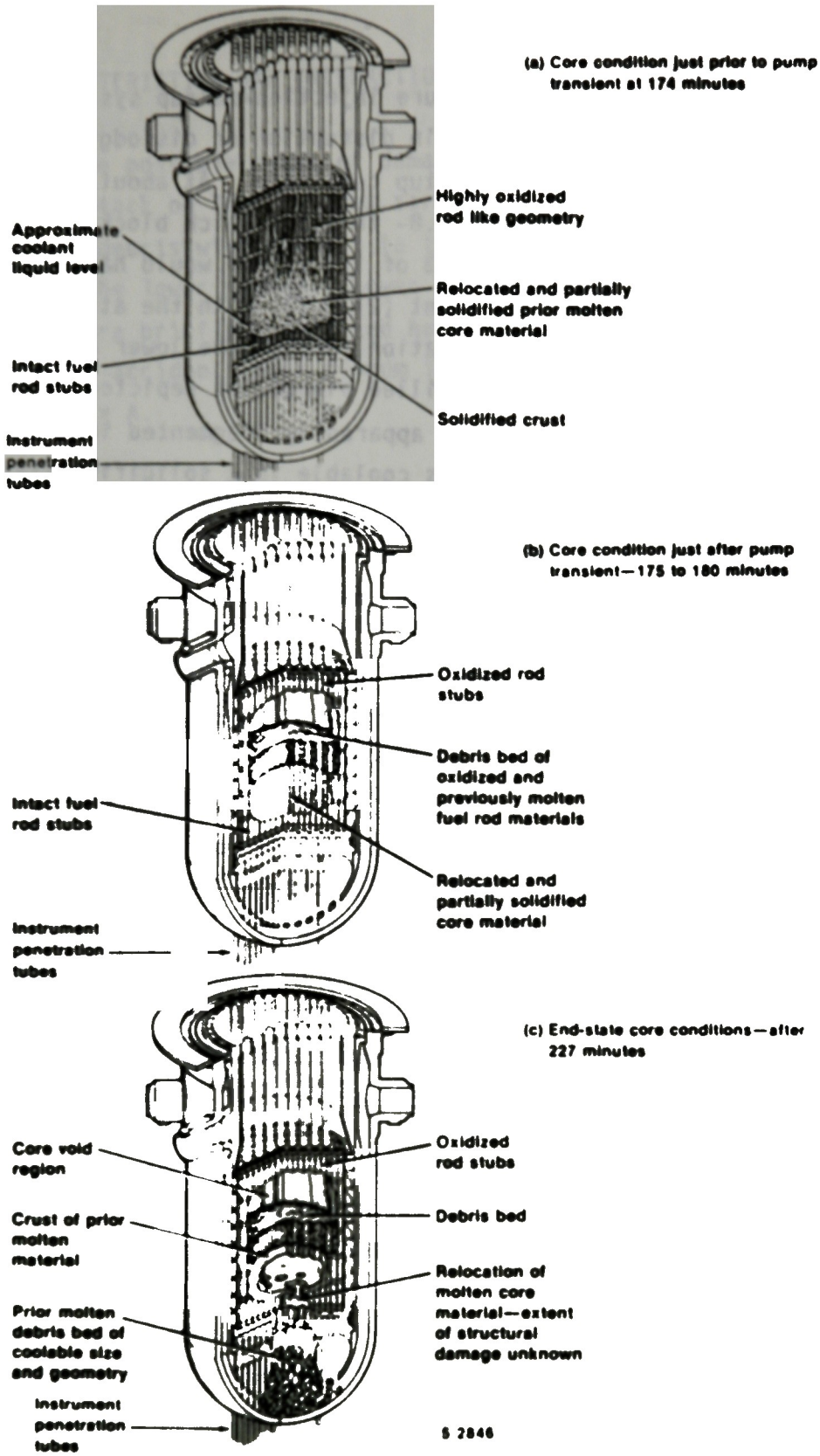

Figure 1. Hypothesized stages of the TMI-2 accident progression.

Actuation of the high-pressure injection/makeup system (HPIS) at 200 min probably did not result in disruption or dislodging of the blockage to any great extent, so that heatup continued. At about 220-230 min, SCDAP predictions[2] indicate that the 0.8- to 1.5-m-thick blockage region would have heated to the point that 2/3 of its volume would have exceeded the α-Zr(O)/UO_2 eutectic melting point (2170 K), with the attendant initiation of downward melt migration through the lower core support and flow structures into the water-filled plenum, as depicted in Figure 1c. Upon impact with water, the melt apparently fragmented into a debris size sufficiently small so that it was coolable in a solidified state. Thus, melt progression was probably terminated by the presence of water in the lower plenum, which protected the lower head from direct melt attack. The core debris thus finally attained a coolable state.

The above scenario is somewhat speculative at this time and will require confirmation or refinement via an on-going comparison of analysis with TMI-2 vessel inspection and core removal efforts. Nevertheless, it does point to the principal concerns of interest here, namely, debris coolability in the lower plenum and potential for thermal attack by the hot debris on the lower vessel head and attached instrument penetration tubes. In the following section, a brief overview is presented of known conditions of the lower plenum and debris, obtained from various TMI-2 vessel inspection efforts. These data are used to assess debris thermal interaction potential with lower plenum structures. Conclusions are then drawn relative to the potential damage state of the lower plenum.

DEBRIS CHARACTERISTICS AND INTERACTION WITH LOWER PLENUM STRUCTURES

To assess the possible range of damage consequences due to potential debris thermal attack on lower plenum structures, it is first necessary to characterize the debris with respect to thermal properties and the known damage state of the lower plenum. Lower plenum damage characterization efforts to date are briefly summarized here, based on information obtained from various post-accident lower plenum inspection efforts described in detail in Appendix A.

In September 1983, two axial strings of solid-state neutron track recorders (SSTRs) were installed in the annular gap between the reactor vessel and the biological shield.[7] The resulting axial flux profile differed significantly from what would be expected for a normal core, with significant neutron streaming from fuel in the lower plenum. Predictions indicated that approximately 10 to 20 metric tons of fuel debris may have relocated to this region. Such findings prompted initiation of subsequent video inspections of the lower plenum.

On February 20-22, 1985, and again during July 1985, video inspections of the lower plenum were performed.[8] Figure 2 presents a schematic illustration of the lower plenum configuration and camera view orientation for the debris shown in Figure 3. Estimates of the debris depth range from 25 to 70 cm above the bottom invert of the head. The debris appears to be segregated radially, with the loose sand-to-gravel type material near the center and larger agglomerations up to a few inches in diameter towards the edges. Figure 3 presents a view of the debris bed in the region of the Inconel penetration nozzle and stainless steel guide tube junction. Although the Inconel penetration nozzle is shown to be intact above the surface of what appears to be a rather densely packed debris bed, this may not be the case below the debris surface where coolant in-penetration may have been limited. Thus, the question arises as to the physical state of the Inconel penetration nozzles with a melting point of ≈1615 K.

ANALYSIS OF THERMAL ATTACK OF DEBRIS ON PENETRATION NOZZLES AND LOWER HEAD

The lower plenum contains several structural components which would experience thermal attack by hot debris, including the head and the bottom-entry penetration tubes. Thermal degradation of the penetration tubes and lower head is considered in this section, since these structures are of primary concern for evaluating the mode and timing of vessel failure.[13,14]

As discussed in Reference 15, for coherent large-scale debris migration to the lower plenum, the water would be either displaced by the debris or vaporized. For such large mass discharge, molten or solid debris would most likely penetrate to the bottom of the plenum, where it could accumulate and cause thermal attack on the lower head and bottom-entry instrument penetration tubes. For more limited debris migration, quenching of debris may be possible. The latter situation apparently was achieved at TMI-2, since the lower head forging remained intact. Although vessel integrity was maintained at TMI-2, nevertheless the question arises as to the damage state of the lower plenum. An assessment of this question primarily centers on the ability to reconstruct the penetration tube and lower head temperatures reached during the accident, which are addressed here.

Thermal Analysis of Penetration Tubes

Both Babcock & Wilcox (TMI-2) and Westinghouse PWRs contain instrument penetration tubes through the lower head, which serve as entry ports for neutron flux monitors and other in-core instrumentation. Because of the large number of penetrations (52 for TMI-2) and the three-dimensional nature of thermal attack that these tubes would experience (as opposed to essentially one-dimensional heat transfer in the more massive vessel head), such penetrations could be subject to early failure and the attendant potential to duct core material from the pressure vessel to the containment.

As indicated in Appendix A, each bottom-entry instrument penetration is essentially continuous tubing, which starts from an instrument panel located in the containment building above the top of the reactor vessel. The access path is downward through the instrument tunnel and reactor cavity, turns upward below the reactor vessel, and penetrates the reactor vessel through holes in the lower head forging, being sealed to the head by welding brazements. In-core instruments are inserted into the vessel through these tubes and are indexed by a switching device so that the neutron flux and temperature distribution within the core can be mapped.

A cross-sectional view of an inserted in-core TMI-2 detector assembly is given in Appendix A (Figure A-8). Each assembly consists of seven self-powered neutron detectors (SPNDs), one background sensor, and one thermocouple. The SPNDs, background sensor, thermocouple, and spacer tube form a movable detector housed in an Inconel oversheath surrounded by water within the instrument tube. The instrument assembly first penetrates the reactor vessel through an Inconel penetration nozzle ~12 in. long above the inside surface of the lower head. The penetration nozzle then fits into a stainless steel guide tube, which guides the instrument assembly through the lower plenum structures (i.e., flow distributor plate, core support plate, lower grid forging, etc.) into the core proper. The instrument string itself consists of a double-walled configuration with an internal water jacket. A more detailed description of the instrument assembly is given in Appendix A.

Figure 4 illustrates the geometry of an instrument penetration nozzle subject to thermal attack by core debris. A feature contributing to the failure potential is the "fin effect" of tube stubs surrounded by hot debris. Likewise, the temperature of the weld material at the penetration-head junction would increase faster than the vessel wall itself, since the penetration nozzle acts as a conduction path for heat transport from the debris to the welds. Consequently, the penetration junctions can be expected to fail before the lower head. An evaluation of core debris thermal attack on the TMI-2 penetration nozzles is presented here, using the debris characteristics defined in the previous section.

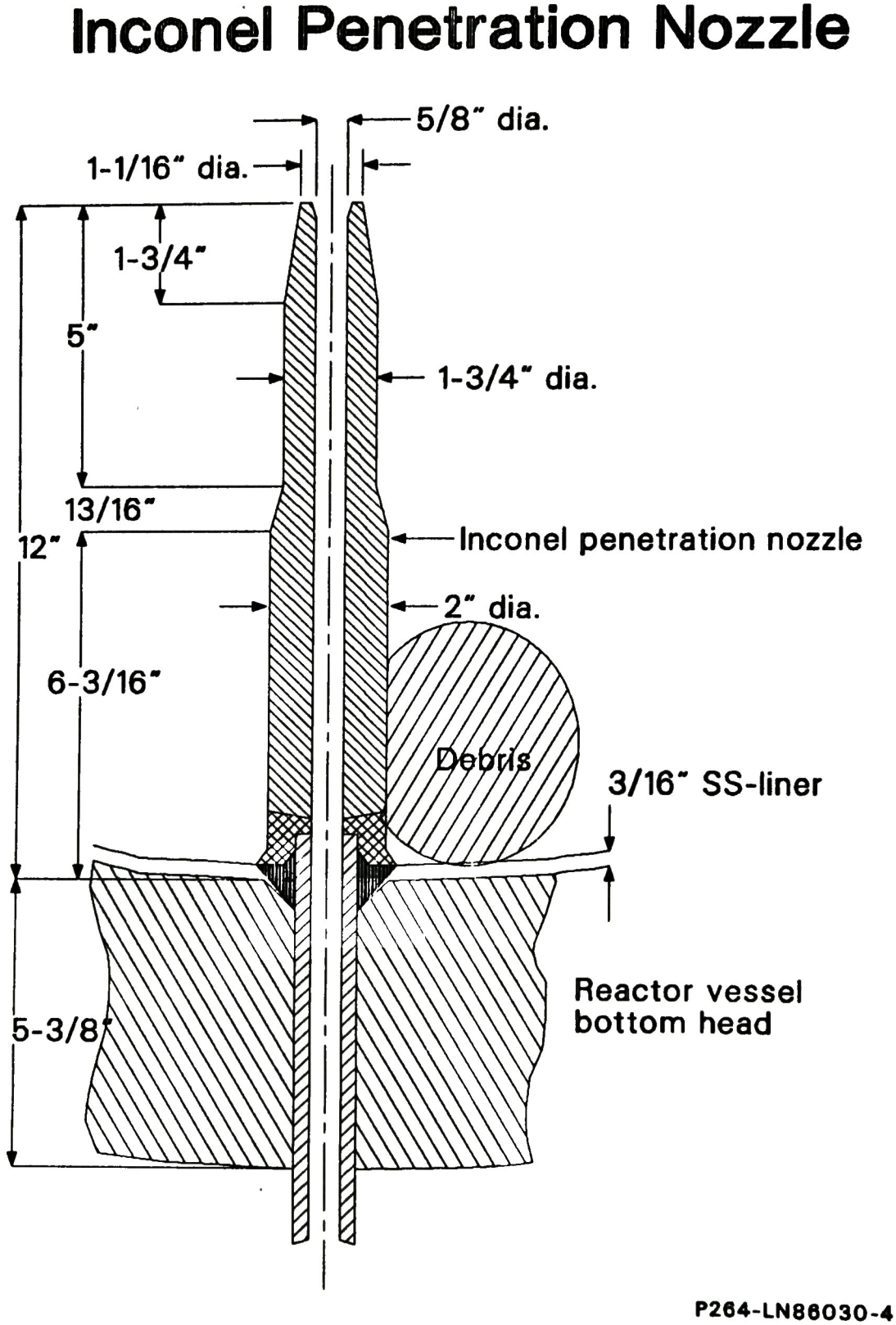

Figure 4. Illustration of bottom-entry TMI-2 instrument penetration configuration.

Melt Failure Potential of Penetration Nozzle

The thermal response of the Inconel penetration nozzle just above the vessel head is investigated with respect to attack by hot corium debris, based upon the configuration illustrated in Figure 4. It is important to note that the geometry illustrated in Figure 4 and the analysis presented here are idealized with respect to debris thermal attack on the penetration nozzle, where the timing and conditions leading to potential nozzle melt failure are of interest. As such, the configuration investigated is one of a tightly packed debris bed, with essentially no coolant ingress into the bed in the vicinity of the penetration nozzle. For the additional assumption that the inside surface of the nozzle may be subject to adiabatic heating due to loss of coolant entry by debris blockage, the thermal relaxation time, t_t,[a] of the nozzle wall thickness (X = 1/2 [2.0 - 0.625] in.) can be estimated as:

$$t_t = \frac{X^2}{4\alpha} \tag{1}$$

where α = thermal diffusivity. Using Inconel properties (see Table 1), the time period for thermal penetration is estimated in Table 2 to be ~22 s. If the heat of fusion for nickel (the main component of Inconel) is taken into account, the thermal relaxation time for melting ($t_{t,m}$) can be approximated as:[16]

$$t_{t,m} = \frac{X^2}{4\alpha\, a^2} \tag{2}$$

where a is the dimensionless solidification constant, which can be approximated as:

$$\frac{C_p\, T_{mp}}{L(\pi)^{0.5}} = a \exp(a^2) \tag{3}$$

---

a. The thermal relaxation time can be defined as the time period for a temperature perturbation at the surface of a heat-conducting body to be conducted to some interior position.

TABLE 2. CALCULATION OF THERMAL RELAXATION TIME FOR INCONEL PENETRATION NOZZLE

Nozzle Dimensions:

OD = 2.0 in.

ID = 0.625 in.

Thickness = 1/2 [2.0 - 0.625] = 0.6875 in.

Thermal Relaxation Time:

$$t_t = \frac{X^2}{4\alpha}$$

X = 0.6875 in.

$$\alpha = 0.1368 \frac{ft^2}{h} \times \frac{h}{3600\ s} \times \frac{144\ in^2}{ft} = 5.47(10^{-3})\ in^2/s$$

$$t_t = \frac{(.6875)^2}{4(5.47 \times 10^{-3})} = 21.6\ s$$

For Inconel melting, the solidification constant is estimated in Table 3 to be approximately 0.7. Using this value, nozzle failure due to melting is indicated to occur in less than 1 min. Thus, for localized hot-spot regions, nozzle melt-through could occur rather quickly, if the debris temperature exceeds the Inconel melting point of ~1615 K.

To assess in an approximate manner the debris temperature and particle size conditions that would lead to a debris-Inconel contact temperature exceeding the Inconel melting point of 1615 K, the steady heat-conduction equation for spherical geometry with an internal heat source was investigated, i.e.:

$$\frac{1}{r^2}\frac{d}{dr}\left(r^2 k \frac{dT}{dr}\right) = -q''' \qquad (4)$$

where k = thermal conductivity, r = radial position, and q''' = volumetric heat generation rate. Assuming constant properties, the solution is:

$$T(r) = T_s + \frac{q'''}{6k}(R^2 - r^2) \qquad (5)$$

where R = debris radius and T_s = debris surface temperature. Using the TMI-2 burnup condition and a 5 h decay-period, q''' is estimated to be 10^6 W/m^3, while an effective conductivity of 5 W/m-K is assumed for ceramic-type debris.

Efficient heat transfer can be expected for good debris-nozzle contact due to the relatively high conductivity of the Inconel heat sink material. The particle size/temperature conditions for penetration nozzle failure via surface melting/ablation can therefore be assessed by using a debris surface temperature, T_s, equal to the Inconel melting point (1615 K). For debris breakup to particle diameters, D_p, equal to or less than the 6-in. (0.152-m) diameter holes of the lower flow distributor, the debris center temperature, T_o, necessary to maintain a debris surface temperature of 1615 K is estimated in Table 4 at various particle diameters, i.e.:

D_p = 1 in. (0.0254 m) $T_o \simeq 1620$ K
D_p = 4 in. (0.1016 m) $T_o \simeq 1700$ K
D_p = 6 in. (0.152 m) $T_o \simeq 1810$ K

Since the eutectic melting point of UO_2/α-Zr(O) is about 2170 K,[17] the debris need not be molten to cause surface melt ablation of the penetration nozzles. In other words, debris particles smaller than the hole size of the flow distributor can be in a solid condition and still cause surface melting of the Inconel penetration nozzles. Such analysis indicates that nozzle failure may have occurred at local regions of solid debris/nozzle contact, if the debris bed were in a localized noncoolable configuration.

As discussed in Appendix A, uncertainty exists as to the exact composition of the debris in the lower plenum. In the above calculation, the debris was assumed to be composed primarily of heat generating fuel, with a thermal conductivity representative of ceramic UO_2. However, the initial gamma probing studies indicate that the debris may be composed primarily of structural or control rod material rather than fuel.[10] Equation 5 was therefore reevaluated assuming a particle conductivity equal to that of stainless steel (k = 16 W/m-K) and a reduction in heat generation rate by an order-of-magnitude to 10^5 W/m^3. The center temperature, T_o, of mostly structural debris for a surface temperature equal to the Inconel melting point (T_s = 1615 K) is estimated in Table 5, where results can be summarized as follows:

D_p = 1 in. (0.0254 m) $T_o \simeq 1615$ K
D_p = 4 in. (0.1016 m) $T_o \simeq 1618$ K
D_p = 6 in. (0.152 m) $T_o \simeq 1621$ K

As indicated for high conductivity metallic-like debris, the debris temperature need not be much above the Inconel melting temperature (1615 K) to cause surface melt ablation of the penetration nozzle.

TABLE 5. CALCULATION OF PARTICLE TEMPERATURE GRADIENT ASSUMING METALLIC CORE DEBRIS IN TMI-2

Governing Equation:

$$T_o = T_s + \frac{q'''}{6k} R^2$$

Parameter Values:

$T_s = T_{mp}$(Inconel) = 1615 K

$q''' = 10^5$ W/m^3 $\qquad \frac{q'''}{6k} = 1.04(10^3)$ K/m^2

$k = 16$ W/m-K

Calculation:

D_p	R	$\frac{q'''}{6k} R^2$	T_o
1 in. (0.0254 m)	0.0127 m	0.17 K	≈1615 K
4 in. (0.1016 m)	0.0508 m	2.69 K	≈1618 K
6 in. (0.1524 m)	0.0762 m	6.05 K	≈1621 K

In the above analysis, it was assumed that good nozzle-debris contact exists and that heat transfer conditions are such that the melting temperature of Inconel (1615 K) is reached at the plane of contact. This situation can only exist for degraded cooling at the inside of the penetration nozzle (i.e., boiloff of entrapped coolant) and for debris which has sufficient sensible heat to raise the nozzle wall material to the Inconel melt temperature. To assess if such thermal conditions are possible, a heat balance is written for a segment of the penetration nozzle (heat sink) and the associated debris heat source in immediate contact with the nozzle. In such analysis, an assessment is made of the debris size and temperature conditions necessary to raise the penetration nozzle wall thickness to the Inconel melting point (1615 K), where a heat balance is performed using the following expressions:

$$\text{Sensible heat of debris particle} = \left(\frac{\pi D_p^3}{6}\right)(\rho C_p)(T_{p,o} - 1615) \tag{6}$$

$$\text{Sensible heat of nozzle wall thickness} = \left(\frac{\pi D_p}{4}\right)[OD^2 - ID^2](\rho C_p)[1615 - T_{n,o}] \tag{7}$$

$$\text{Latent heat of nozzle wall thickness} = \left(\frac{\pi D_p}{4}\right)[OD^2 - ID^2](\rho L) \tag{8}$$

where

L = the latent heat of fusion

$T_{p,o}$ = the initial debris temperature

$T_{n,o}$ = the initial nozzle temperature, which is taken as the saturation temperature of water at 1500 psi (i.e., 596°F = 586 K)

D_p = the debris diameter and the height of the nozzle associated with each debris particle

T_s = the melting point of Inconel = 1615 K.

Equating the sensible heat given up by the debris to the sensible heat gain and heat of fusion needed for melting of the penetration nozzle thickness, the debris temperature for nozzle melting can be expressed as:

$$T_{p,o} = 1615\ K + \frac{3\,[OD^2 - ID^2]\,\rho_{wall}}{2\,D_p^2\,(\rho C_p)_{debris}}\,[C_{p,\,wall}\,(1029\ K) + L] \qquad (9)$$

Table 6 presents calculational results where the stainless steel debris size and temperature conditions leading to nozzle melting are estimated, which can be summarized as:

D_p = 4 in. (10.16 cm)	$T_{p,o}$ = 2122 K
D_p = 6 in. (15.24 cm)	$T_{p,o}$ = 1840 K

Since the melt temperature of stainless steel is 1640 K, a molten steel inventory on the order of 4 to 6 in. in diameter must be 200 to 400 K above its melting point to cause adiabatic nozzle wall heating to a melt condition. Thus, heat-generating fuel debris would result in nozzle melting at temperatures lower than those assuming structural debris (with no decay heat source).

Such analysis indicates that melt failure of the penetration nozzle by debris contact could have occurred during the TMI-2 accident at local noncoolable regions of the debris bed. If, however, the debris bed were homogeneously coolable, then such hot-spot regions would not have existed and penetrations would have remained intact. However, results of the wire probing studies discussed in Appendix A indicate damage or plugging of the penetration nozzles at approximately 5 to 20 ft below the base of the reactor. Such plugging may be due to debris entry into the nozzle or freezing of Inconel melt as it flows downward through the penetration tube. An assessment of the depth of melt flow within the penetration lead tube is presented next.

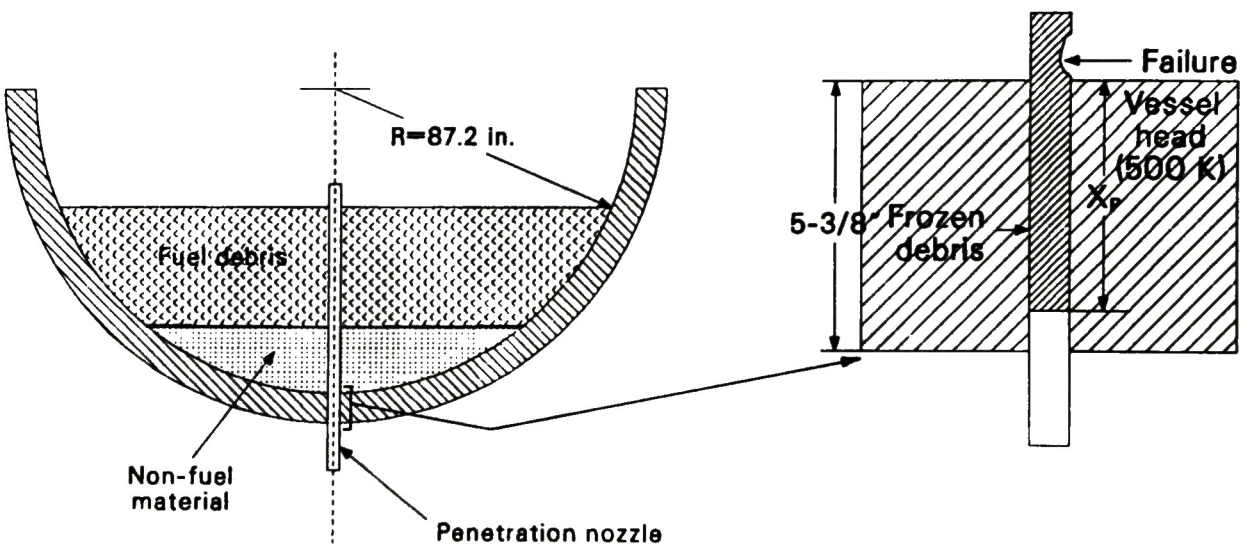

Figure 5. Illustration of the downward penetration of TMI-2 fuel debris through an Inconel instrument nozzle and refreezing in a cooler region.

up by an element of molten fuel of diameter D, length ΔX, initial temperature T_o, velocity U, specific heat C_p, and latent heat of fusion L_f, upon cooling to the solid state can be expressed as:

$$\frac{\pi}{4} D^2 \rho_f (\Delta X)[C_p(T_o - T_{mp}) + L_f] = Q_f \qquad (10)$$

where T_{mp} is the melting point. The sensible and latent heat given up to the wall, Q_w, can be expressed in terms of the heat transferred by turbulent convection over the fuel melt penetration distance X_p, i.e.:

$$\pi D(\Delta X)h(T_o - T_w)\, X_p/U = Q_w$$

where h is the turbulent heat-transfer coefficient and T_w is the wall temperature of the channel. Equating Q_f to Q_w, the penetration distance, X_p, for plug freezing can be expressed as:

$$X_p = \frac{1}{4} \frac{UD\rho_f C_p}{h} \left[\frac{L_f/C_p + (T_o - T_{mp})}{T_o - T_w}\right] \qquad (11)$$

In deriving the above equation, changes in the mean temperature of the molten fuel have been neglected as the melt proceeds along the channel, which is a valid approximation providing $(T_o - T_{mp})/(T_o - T_w) \ll 1$.

The above equation for X_p can be further simplified[19] by elimination of the heat transfer coefficient, h. Assuming that turbulent heat transport within the channel is well represented by the Reynolds' analogy, which provides a linear relationship between the heat-transfer coefficient h and the frictional shear stress S, it can be seen that

$$h = C_p \frac{S}{U} = C_p \frac{f\rho_f U^2}{2U} = \frac{f}{2} \rho_f C_p U \qquad (12)$$

where f is the dimensionless coefficient of friction, which is estimated in Appendix B for present conditions to be on the order of $f \simeq 0.023$. Combining the above equations leads to the following simple expression for the penetration distance, X_p, freezing of a melt slug in a cold channel:[19]

$$X_p = \frac{D}{2f} \left[\frac{L_f/C_p + (T_o - T_{mp})}{T_o - T_w}\right] \tag{13}$$

Calculational results for Cases A, B, and C are presented in Tables 7, 8, and 9 respectively. As indicated, molten material in all cases (i.e., for a range of wall temperatures from 100°F to 1000°F) is predicted to freeze at a penetration length of less than 2 ft, while the wire probing studies indicate plugging an average of about 10 ft from the bottom of the reactor vessel. It should be noted, however, that the predicted plugging distance is largely affected by the accuracy of the friction factor (i.e., an indirect linear dependence) which is highly uncertain. A decrease in f by a factor of 5 to 10, which is within the range of uncertainty, would result in a predicted plugging distance of similar magnitude as the probe data. On comparing Tables 7, 8, and 9, it can be seen that the largest depth of melt penetration is for the low-melting-point control rod material (T_{mp} = 1470°F). Wall melt failure of the penetration nozzles within the reactor vessel, with refreezing of melt debris below the reactor head, is therefore a predicted possibility.

In the above analysis, it was assumed that the melt debris within the breached penetration nozzle occupies the entire cross-sectional area. However, in general, the instrument string is inserted within the penetration nozzle, so that the more likely configuration for melt drainage is within the annulus between the nozzle wall (ID = 0.625 in.) and that of the instrument assembly (OD = 0.292 in.). The hydraulic diameter, D_h, for this annulus can be approximated as:

TABLE 7. PENETRATION DISTANCE FOR REFREEZING OF MOLTEN INCONEL

Governing Equation:

$$X_p = \frac{D}{2f}\left[\frac{L_f/C_p + (T_o - T_{mp})}{T_o - T_w}\right]$$

Parameter Values:

L_f = 128 B/lb

C_p = 0.106 B/lb-°F

f = 0.023 (see Appendix B)

D = 5/8 in. = 0.625 in. = 0.052 ft

T_{mp} = 2450°F

D/2f = 1.13 ft

L_f/C_p = 1207°F

$\Delta T_f = T_o - T_{mp}$

Calculation:

ΔT_f, °F	T_o, °F	T_w, °F	X_p, ft
50	2500	100	0.59
50	2500	300	0.64
50	2500	500	0.71
50	2500	1000	0.91
100	2550	100	0.60
100	2550	300	0.66
100	2550	500	0.72
100	2550	1000	0.95
300	2750	100	0.64
300	2750	300	0.69
300	2750	500	0.76
300	2750	1000	0.97

TABLE 8. PENETRATION DISTANCE FOR REFREEZING OF MOLTEN UO_2

Governing Equation:

$$X_p = \frac{D}{2f}\left[\frac{L_f/C_p + (T_o - T_{mp})}{T_o - T_w}\right]$$

Parameter Values:

L_f = 278 J/kg = 119 B/lb

C_p = 33 cal/mole-K = 0.12 B/lb-°F

f = 0.023 (see Appendix B)

D = 0.052 ft

T_{mp} = 3150 K = 5210°F

D/2f = 1.13 ft

L_f/C_p = 992°F

$\Delta T_f = T_o - T_{mp}$

Calculation:

ΔT_f, °F	T_o, °F	T_w, °F	X_p, ft
50	5260	100	0.23
50	5260	300	0.24
50	5260	500	0.25
50	5260	1000	0.28
100	5310	100	0.24
100	5310	300	0.25
100	5310	500	0.26
100	5310	1000	0.29
300	5510	100	0.27
300	5510	300	0.28
300	5510	500	0.29
300	5510	1000	0.32

TABLE 9. PENETRATION DISTANCE FOR REFREEZING OF MOLTEN SILVER-INDIUM-CADMIUM

Governing Equation:

$$X_p = \frac{D}{2f}\left[\frac{L_f/C_p + (T_o - T_{mp})}{T_o - T_w}\right]$$

Parameter Values:

L_f = 26.5 cal/g = 46.8 B/lb

C_p = 250 J/kg-K = 0.06 B/lb-°F

f = 0.023 (see Appendix B)

D = 5/8 in. = 0.625 in. = 0.052 ft

T_{mp} = 1470°F

D/2f = 1.13 ft

L_f/C_p = 780°F

$\Delta T_f = T_o - T_{mp}$

Calculation:

ΔT_f, °F	T_o, °F	T_w, °F	X_p, ft
50	1520	100	0.66
50	1520	300	0.77
50	1520	500	0.92
50	1520	1000	1.80
100	1570	100	0.68
100	1570	300	0.78
100	1570	500	0.93
100	1570	1000	1.74
300	1770	100	0.73
300	1770	300	0.83
300	1770	500	0.96
300	1770	1000	1.58

$$D_h = 4 \left(\frac{\text{Cross-Sectional Flow Area}}{\text{Wetted Perimeter}}\right) = 4 \left(\frac{A_f}{P_w}\right) \quad (14)$$

$$P_w = \pi\,[0.625 + 0.292] = \quad [0.917] \text{ in.}$$

$$A_f = \frac{\pi}{4}\,[(0.625)^2 - (0.292)^2] = \frac{\pi}{4}\,[0.3054] \text{ in.}^2$$

$$D_h = 0.333 \text{ in.}$$

Note that the hydraulic or equivalent diameter can be used to replace the open diameter in correlations for the prediction of heat transfer coefficients and that D_h (0.333 in.) is about half the diameter of an open nozzle (ID = 0.625 in.). The penetration distance, X_p, assuming annular flow, would be about half that predicted in Tables 7, 8, and 9, due to the linear dependence of X_p on the diameter.

If core debris penetrates below the reactor head, then the question arises as to whether the Inconel lead tube connected to the penetration nozzle can be breached by the presence of hot debris. Figure 6 illustrates the general features of the problem, where radiation heat transfer from the outside surface of the tube to the concrete wall of the containment well through an air atmosphere is considered the primary mode of surface cooling, which can be represented by the following equation:

$$Q_R = A_s \sigma \varepsilon \,(T_s^4 - T_a^4) \quad (15)$$

where

A_s = surface area for heat transfer

Q_R = rate of heat transfer by radiation, B/h

σ = Stefan-Boltzmann constant, $0.1714(10^{-8})$ B/h-ft^2-R^4

ε = effective emissivity ≈0.2 (assumed)

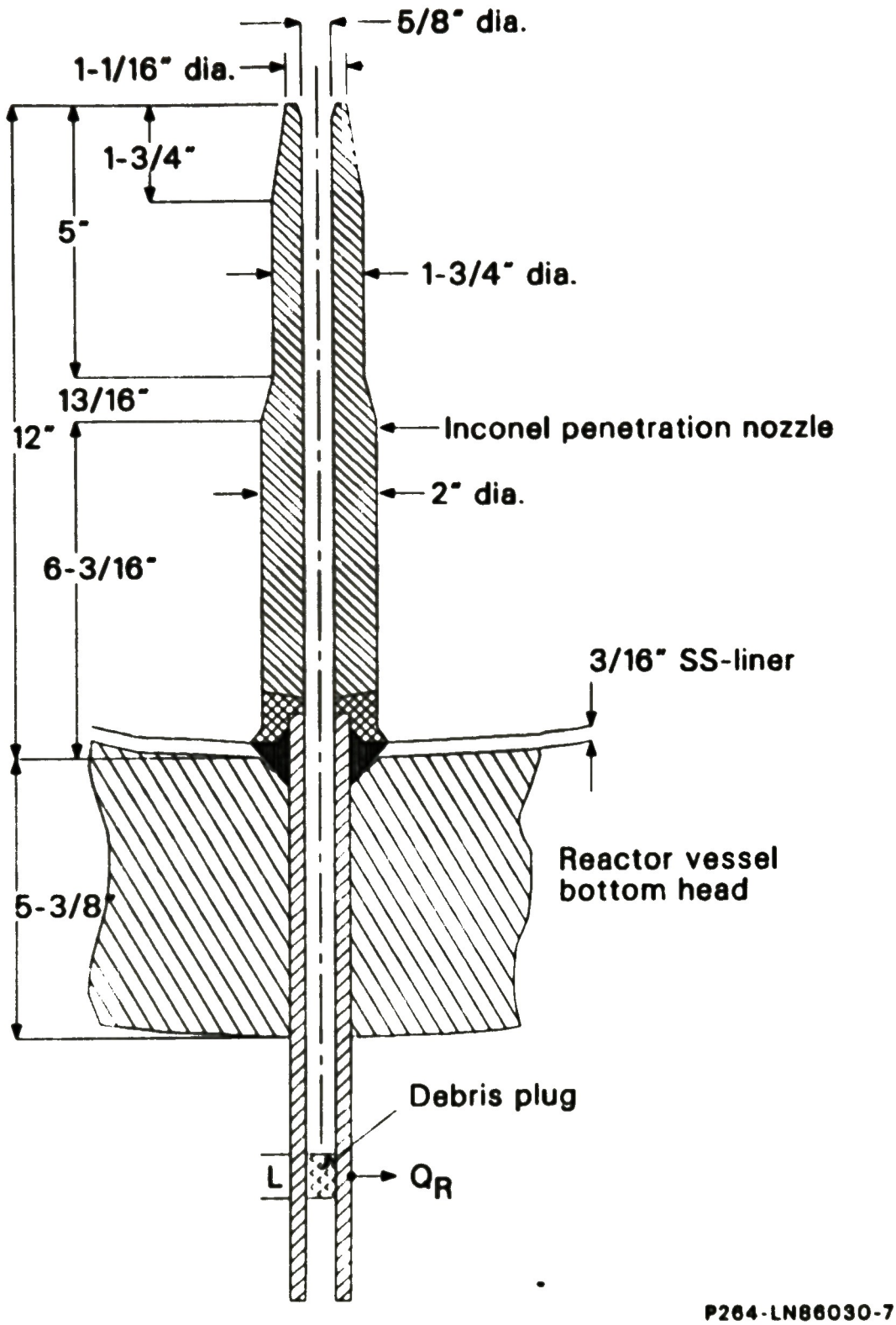

Figure 6. Illustration of radiation heat transfer from TMI-2 core debris plugged within a penetration lead tube.

T_s = tube surface temperature, R

T_a = containment well temperature ≈140°F = 600 R (assumed)

Assuming steady-state heat transfer, equating the volumetric heat source Q ($B/h\text{-}ft^3$) of the debris to Q_R, and using the appropriate system dimensions,

$$A_s = L\pi(OD) \tag{16}$$

$$Q_R = Q\left[\frac{L\pi(ID)^2}{4}\right] \tag{17}$$

so that the tube outside surface temperature can be expressed as:

$$T_s = \left[T_a^4 + \frac{Q\,(ID)^2}{4\,(OD)\,\sigma\epsilon}\right]^{0.25} \tag{18}$$

Calculational results are presented in Table 10 indicating an outside surface temperature of the penetration tube of approximately 760°F, while the melting point of Inconel is 2450°F. Therefore, stable plugging of the penetration tubes by core debris is predicted, which is in agreement with the TMI-2 wire probe findings of intact penetration lead tubes which are blocked below the reactor pressure vessel.

In the above analysis, it was assumed that the melt debris within the breached penetration tube occupies the entire cross-sectional area. However, if the instrument string is accounted for, then the actual cross-sectional area occupied by fuel-debris, A_f, is only 0.24 $in.^2$ In this case, the system parameters are:

$$A_s = L\pi(OD) = L\pi(1.05\text{ in}) = L\ (3.3\text{ in}) = L\ (0.275\text{ ft})$$

$$Q_R = QL\ (0.24\text{ in.}^2) = QL\ (0.00167\text{ ft})$$

TABLE 10. ESTIMATE OF TMI-2 PENETRATION LEAD TUBE TEMPERATURE

Governing Equation:

$$T_s = [T_a^4 + \frac{Q\,(ID)^2}{4\,(OD)\,\sigma\epsilon}]^{0.25}$$

Parameter Values:

T_a = 140°F = 600 R

$$Q = \frac{10^6 W}{m^3} \times \frac{3.414\ B/h}{W} \times \frac{1\ m^3}{35.3\ ft^3} = 9.67\ (10^4)\ B/h\text{-}ft^3$$

σ = 0.1714 (10^{-8}) B/h-ft^2-R^4

ϵ = 0.2 (assumed)

ID = 0.625 in (Fig. 3-8) = 0.052 ft

OD = 1.05 in (Fig. 3-8) = 0.0875 ft

$$\frac{Q\,(ID)^2}{4\,(OD)\,\sigma\epsilon} = 2.096\ (10^{12})\ R^4$$

Calculation:

$T_s = [(600)^4 + 2.096\ (10^{12})]^{0.25}$ = 1220 R

T_s = 760°F

so that a lower surface temperature is predicted due to a lower volumetric heat source, that is,

$$T_s = \left[T_a^4 + \frac{Q\,(0.00167)}{\sigma\varepsilon\,(0.275)}\right]^{0.25} \tag{19}$$

$$T_s = \left[(600)^4 + 1.7(10^{12})\right]^{0.25} = 1165\ R = 705°F$$

The above analysis assumes gravity flow of the melt debris, based on the fact that the instrument penetration tube is pressure-sealed up to the containment access tube (see Figure A-9). This assumption is valid as long as the penetration lead tube remains intact, which apparently is the case for the TMI-2 reactor. However, should the lead tube be breached outside the reactor, pressure equilibrium can no longer be assumed; so that melt drainage would be affected by the differential pressure between the reactor and the containment building. If this were true, then forced melt flow through the penetration tubes would tend to ablate the tube and subsequently the steel vessel head, resulting in an increased opening to duct melt debris from the vessel.[15] The fact that there is no indication of the presence of core debris in the containment building reactor cavity is indirect evidence of the maintenance of penetration lead tube integrity outside the pressure vessel.

Observations Regarding Damage State of Penetration Nozzles

From synthesis of the lower plenum debris data obtained to date and the thermal analysis presented above, the following observations are made relative to the damage state of the instrument nozzles protruding through the lower head. Of prime importance is the fact that debris composed of fuel with a decay heat source need not be in a molten state in order to cause melt failure of the nozzle. This is due to the fact that the nozzle is made of relatively low-melting-point Inconel (T_{mp} = 2450°F, 1616 K). It should be noted that the primary design criterion for the instrument nozzles is their capability to withstand high system pressures, rather than melt attack by core debris. Noting that the yield strength for Inconel at

600°F is on the order of 40,000 psi and that the nozzle tube dimensions are OD = 2.0 in. and ID = 0.625 in., it can be seen from shell theory that the nozzle is capable of withstanding high system pressures, but only at low temperatures. However, the thin wall thickness of the nozzle is subject to melt failure (or creep rupture failure near the melting point) should contact occur with hot core debris in a noncoolable configuration.

Analysis indicates that the debris containing a heat source (fission products) need not be molten to cause melt or creep failure of the Inconel tube wall. The distinct possibility therefore exists for melt failure of the penetration nozzles within the reactor vessel at locations of good debris/nozzle contact. This would be particularly true at locations within the lower plenum of a close-packed debris, where coolant in-penetration may have been limited.

In the calculation of melt penetration, refreezing distances on the order of 1-10 ft were predicted, where uncertainties are largely dependent upon assumptions regarding the wall friction factor, f. Within the uncertainty limits of f, the predicted plugging distance is of the same order of magnitude as the blockage data. Therefore, wall melt failure of the penetration nozzles within the reactor vessel, with refreezing of melt debris below the outside surface of the reactor head, is indeed a distinct possibility. Stable plugging within the penetration lead tubes is also predicted, based upon a steady-state assessment of the tube wall temperature subject to radiation heat transfer to the containment atmosphere. Stable plug freezing is also in agreement with the TMI-2 wire probe findings.

Thermal Analysis of the Lower Head

Although melting of the thin-wall penetration nozzles is the likely failure mode for reactors which incorporate bottom-entry instrumentation, massive sudden molten core debris collapse into the lower plenum could also cause catastrophic vessel wall failure by melt ablation. An assessment of

the potential for such vessel head melting is presented here, based upon an estimate of the instantaneous temperature at the head surface upon initial contact with molten core debris.

Instantaneous Contact Temperature

As discussed in Reference 15, for coherent massive debris migration to the lower plenum, the water would most likely be either displaced by the debris or vaporized. For such coherent large-mass discharge, the molten debris would most likely penetrate to the bottom of the plenum, where it could accumulate and begin to thermally attack the steel surfaces in this locale. The plenum water may continue to vaporize off the upper surface of the debris, but this may not substantially affect the rate of attack on the vessel head.

The configuration of initial molten debris contact with the lower head is shown in Figure 7. To assess if surface melting of the stainless steel liner on the inside surface of the reactor vessel will occur, the following expression for the instantaneous contact interface temperature for two semi-infinite slabs is used,[20] i.e.,

$$T_I = \frac{T_H (k/\alpha^{0.5})_H + T_c (k/\alpha^{0.5})_c}{(k/\alpha^{0.5})_H + (k/\alpha^{0.5})_c} \qquad (20)$$

where

T = temperature
k = thermal conductivity
α = thermal diffusivity
H = hot material (debris)
c = cold material (reactor vessel)

Calculational results are presented in Table 11, where it can be seen that due to the higher conductivity of the vessel wall as compared to the core debris the interface temperature is closer to the bulk temperature of

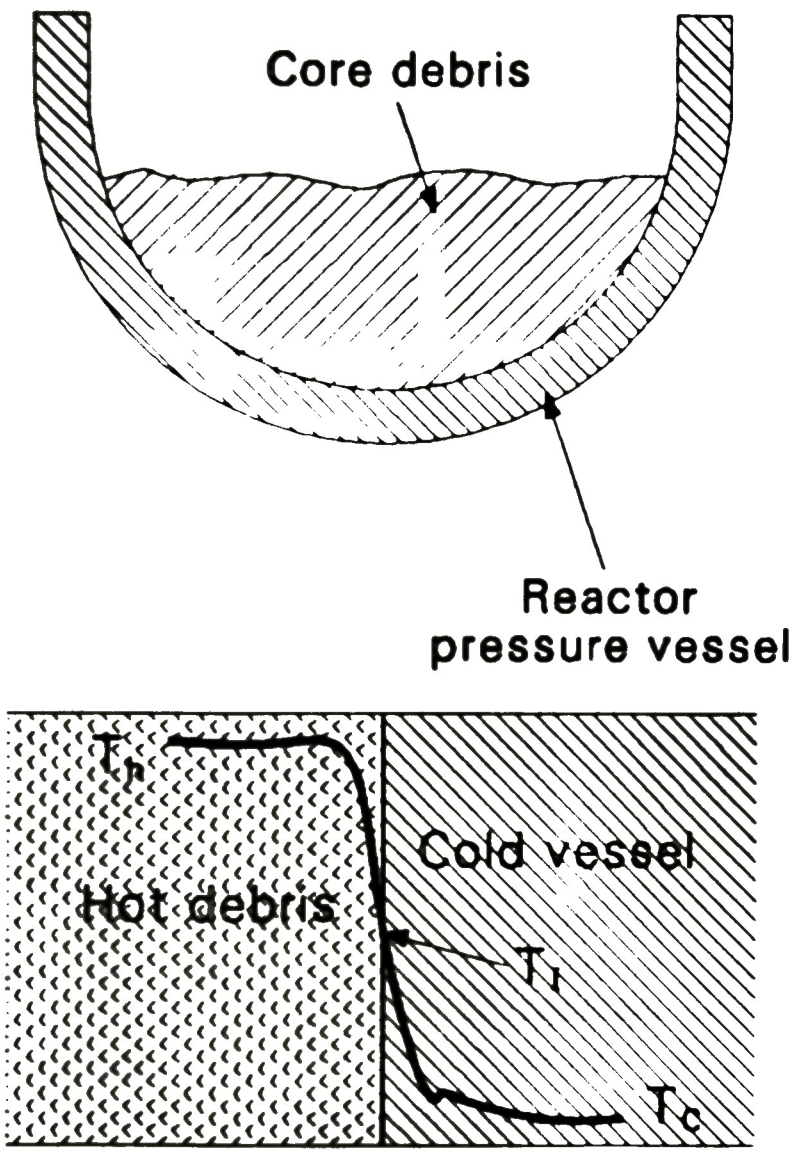

Figure 7. Illustration of bottom-head thermal attack by hot TMI-2 core debris.

TABLE 11. ESTIMATE OF CONTACT INTERFACE TEMPERATURE BETWEEN UO_2 DEBRIS AND TMI-2 VESSEL HEAD

Governing Equation:

$$T_I = \frac{T_H (k/\alpha^{0.5})_H + T_C (k/\alpha^{0.5})_C}{(k/\alpha^{0.5})_H + (k/\alpha^{0.5})_C}$$

Parameter Values:

H = UO_2 Properties	C = Carbon Steel Properties
k_H = 2.1 B/h-ft-°F	k_C = 20 B/h-ft-°f
α_H = 0.032 ft^2/h	α_C = 0.27 ft^2/h
$k/\alpha^{0.5}$ = 11.8	$k/\alpha^{0.5}$ = 38.5
T_{mp} = 5210°F	T_{mp} = 2750°F

Assumption:

Assume vessel head at saturation temperature of water corresponding to a pressure of 1500 lb/in^2; i.e. T_C = 596°F

Calculation:

T_H, °F	T_I, °F
3000	1160
4000	1395
5000	1630
5210	1678
6000	1865

the vessel rather than that of the debris. Since the melting points of the stainless steel liner and carbon steel are 2500°F and 2750°F respectively, melting of either material is not predicted.

Table 12 presents a similar calculation; however, the debris is considered to be a mixture of U-Zr-O components, with an effective metal-like conductivity of 50 W/m-K (28.9 B/h-ft-°F), which is approximately one order of magnitude greater than that of ceramic-UO_2 debris. This increase in debris thermal conductivity (similar for that of Ag-In-Cd alloy) results in an interface temperature which partitions between that of the bulk debris and vessel wall temperatures. Thus, inside surface melting may occur for metallic-like debris temperatures in excess of ~4500°F.

It should be noted that the instantaneous contact temperature is based upon contact between two semi-infinite materials of different properties and bulk temperatures. As such, the solution is valid until a thermal front penetrates the thickness of either, whereupon that material begins to heat up (or cool down), with a corresponding change in interface temperature. Thus, the above estimate is simply an indication of the initial temperature of the inside surface of the vessel head at the time of debris relocation into the lower plenum.

Observations Regarding Damage State of Lower Head

Although no data exist regarding the state of the inside surface of the lower head exposed to TMI-2 core debris, thermal analysis indicates the following trends. For direct contact of core debris with the reactor vessel, the interface contact temperature is predicted to remain well below the melting point of the vessel, if the contacting debris has a thermal conductivity near that of ceramic-like UO_2. For higher conductivity debris, the interface temperature increases, where stainless steel liner melting (T_{mp} = 2500°F) can occur at debris temperatures in excess of ~4500°F (which is about 1000°F above the melting point of α-Zr(O)/UO_2

TABLE 12. ESTIMATE OF CONTACT INTERFACE TEMPERATURE BETWEEN U-ZR-O DEBRIS AND TMI-2 VESSEL HEAD

Governing Equation:

$$T_I = \frac{T_H (k/\alpha^{0.5})_H + T_C (k/\alpha^{0.5})_C}{(k/\alpha^{0.5})_H + (k/\alpha^{0.5})_C}$$

Parameter Values:

H = U-Zr-O Properties	C = Carbon Steel Properties
k_H = 29.0 B/h-ft-°F	k_C = 20 B/h-ft-°F
α_H = 0.45 ft^2/h	α_C = 0.27 ft^2/h
$k/\alpha^{0.5}$ = 43.2	$k/\alpha^{0.5}$ = 38.5
T_{mp} = 2170 K = 3450°F	T_{mp} = 2750°F

Assumption:

Assume vessel head at saturation temperature of water corresponding to a pressure of 1500 lb/in^2; i.e. T_C = 596°F

Calculation:

T_H, °F	T_I, °F
3000	1867
3450	2105
4000	2410
5000	2925
6000	3455

eutectic). However, the larger the fractions of non-fuel material in the debris, the lower its heat generating capacity and thus its temperature. Thus, for direct core debris contact it appears that conditions would not be favorable for rapid melting of the stainless steel liner.

CONCLUSIONS

Based upon data survey efforts of the lower plenum and analysis of thermal interaction between core debris and lower plenum structures, the following observations are summarized relative to the potential damage state of the TMI-2 lower plenum:

- The debris within the lower plenum may contain up to 10 to 20% of the initial loading core material. Video inspection of such debris indicates a debris size ranging from fine sand-like kernels to gravel-like particles up to 2-3 in. in diameter. A retrieval and gross radiation survey of several debris particles indicates a size range of 0.25 to 2.5 in. and that the debris is either primarily structural material or fuel somewhat depleted of fission products. Hydraulic disturbance of the debris shows evidence that the top surface of the debris bed is in a loose rubble configuration. Gamma probing through the L-11 penetration tube indicates that the debris bed may be highly stratified, with a layer of non-fuel material resting on the vessel head with an overlay of ceramic-like fuel debris.

- Wire probing studies of the instrument penetration tubes indicate that 16 of 17 tubes are blocked. The implication of such wire probing is that a large portion of the penetration tubes are either filled with relatively fine debris or damaged by debris thermal attack of the tube walls.

- Thermal analysis indicates melt failure of the Inconel penetration nozzles for either solid ceramic-like fuel debris at temperatures in the range of 1600 to 1800 K, or for metallic-like debris at temperatures greater than 1620 K. Thermal attack by molten stainless steel approximately 200 K above its melting point is also assessed to lead to nozzle melt failure.

- Thermal analysis of the vessel head indicates that the stainless steel liner is not likely to have experienced melting upon sudden contact with either metallic (molten steel or Ag-In-Cd melt) or ceramic fuel debris.

- The likely mode of bottom head failure for severe accidents is assessed to be from debris thermal attack on the bottom-entry Inconel penetration tubes. Melt failure of the penetration nozzles may have occurred at TMI-2. However, melt debris refreezing and plugging in these tubes is predicted, which prevents core material from escaping the reactor vessel.

REFERENCES

1. J. M. Broughton et al., "TMI-2: Core Condition and Postulated Accident Scenario," Trans. Am. Nucl. Soc. (50), 1985, pp. 210-211.

2. C. M. Allison to J. M. Broughton, "Estimate of TMI-2 Core Damage at 174 minutes," CMA-11-85, EG&G Idaho, Inc., August 15, 1985.

3. J. M. Broughton, "Best-Estimate TMI Core Conditions and Accident Scenario," Proc. of the First International Information Meeting on the TMI-2 Accident, CONF-8510166, Germantown, MD, October 21, 1985.

4. S. R. Behling, Computer Code Calculations of the TMI-2 Accident: Initial and Boundary Conditions, EGG-TMI-6859, May 1985.

5. P. Kuan, TMI-2 Core Debris Bed Coolability, EGG-TMI-7150, March 1986.

6. C. M. Allison, E. R. Carlson, and R. H. Smith, "SCDAP: A Computer Code for Analyzing Light Water Reactor Severe Core Damage," Proc. Intern. Mtg. on LWR Severe Accident Evaluation, Cambridge, MA, August 28-September 1, 1983.

7. Technical Planning Department, Determination of Fuel Distribution in TMI-2 Based on Axial Neutron Flux Profile, TPO/TMI-165, Rev. 0, GPU Nuclear Corporation, April 1985.

8. V. R. Fricke, Reactor Lower Head Video Inspection, TMI-2 Technical Planning Bulletin, TPB-85-6, February 26, 1985.

9. D. G. Keefer, "In-Core Instruments Tube Probing," EGG Interoffice Correspondence, April 1, 1985.

10. R. Rainisch, Analysis of Gamma Scanning of In-Core Detector No. 18 L-11 in Lower Reactor Vessel Head, GPU Nuclear Report TPO/TMI-175, June 1985.

11. V. R. Fricke, Hydraulic Disturbance of the Debris in the Bottom Head of the TMI-2 Vessel, TMI-2 Technical Planning Bulletin, TPB-85-20, July 26, 1985.

12. G. Worku, Core Debris Sample Retrieval from the Lower Head Region, TMI-2 Technical Planning Bulletin, TPB-85-21, July 29. 1985.

13. A. W. Cronenberg et al., "Debris Thermal Interaction with Lower Plenum Structures," Proc. of the First International Information Meeting on the TMI-2 Accident, CONF-8510166, Germantown, MD, October 21, 1985.

14. A. W. Cronenberg, S. R. Behling, and J. Broughton, "Analysis of Damage Potential to the TMI-2 Lower Head by Core Debris," Trans. Am. Nucl. Soc. (50), 1985, pp. 217-219.

15. Fauske and Assoc., Inc., Final Report on Debris Coolability, Vessel Penetration, and Debris Dispersal, IDCOR Report Task-15, January 1983.

16. M. S. El-Genk, and A. W. Cronenberg, "An Assessment of Fuel Freezing and Drainage Phenomena in a Reactor Shield Plug Following a Core Disruptive Accident," Nucl. Engr. Design 47, 1978, pp. 195-255.

17. A. Skokan, "High Temperature Phase Relations in the U-Zr-O System," Proc. 5th Intern. Mtg. on Thermal Nuclear Reactor Safety, Karlsruhe, Germany, September 9-13, 1984.

18. R. W. Ostensen, and J. F. Jackson, Extended Fuel Motion Study, ANL-RDP-18, July 1973.

19. M. Epstein et al., "Transient Freezing of a Flowing Ceramic Fuel in a Steel Channel," Nucl. Sci. Engr. (61), 1976, pp. 310-323.

20. A. W. Cronenberg, "Recent Developments in the Understanding of Energetic Molten-Fuel-Coolant Interactions," J. Nucl. Safety (21), 1980, pp. 319-337.

APPENDIX A

TMI-2 DEBRIS CHARACTERISTICS AND INTERACTION WITH LOWER PLENUM STRUCTURES

APPENDIX A

DEBRIS CHARACTERISTICS AND INTERACTION WITH LOWER PLENUM STRUCTURES

In order to assess the possible damage due to thermal attack of core debris on the lower head and bottom entry penetration tubes, it was necessary to characterize the core debris with respect to composition, geometry, and thermal characteristics based on the following primary sources:

- Neutron flux profile,[A-1,A-2]
- Video inspection of the lower plenum,[A-3]
- Wire probing of the instrument penetration tubes,[A-4]
- Gamma-scanning within the lower plenum,[A-5,A-6]
- Probing of the lower plenum debris bed with a high-velocity water jet,[A-7]
- Debris grab-sample retrieval.[A-8]

Each of these efforts is briefly summarized below.

Neutron Flux Profile

In September of 1983,[A-1,A-2] two axial strings of solid-state track recorders (SSTRs) were installed in the annular gap between the TMI-2 reactor vessel and the biological shield. The readings obtained from the SSTRs were used to estimate the thermal neutron flux in the gap. The axial flux profile obtained from the SSTR readings was analyzed using a discrete ordinate transport code and associated neutronic models of the damaged core. Readings differed significantly from what would be expected for a normal core. The analysis showed that the thermal flux profile was

dominated by neutrons streaming from fuel located in the lower vessel head. It was deducted that the magnitude of the thermal flux just outside the vessel at the SSTR string positions was directly proportional to the fuel loading in the lower plenum area. These flux levels were approximately four orders of magnitude above those seen in an undamaged core under the same temperature and boron conditions. This relationship permitted the prediction that approximately 10 to 20 metric tonnes of UO_2 must lie in the lower vessel plenum of the reactor. Such findings prompted initiation of the video inspection effort summarized below.

Video Inspection

On February 20-22, 1985, and again during July 1985, video inspections of the reactor vessel lower head area were performed. A camera was inserted into 3-7/8-in.-diameter holes of the Core Support Assembly (CSA) at several locations shown in Figure A-1. An auxiliary light was inserted down an adjacent hole. The outside surface of the CSA [i.e., the region between the CSA and the inside surface of the reactor vessel (RV)] was inspected on the way down to the bottom head region. The annulus between the CSA and the RV was clean and free of large debris.

The video inspection of the flow distributor plate at the bottom of the CSA showed no evidence of structural damage in any of the areas inspected. There was also no visible damage to the bottom head; however, debris was shown to be covering large portions of the lower head. The tops of the in-core instrument penetration nozzles protruding through the debris stack were shown to be aligned in their normal configuration, indicating no visual damage to the penetration tube above the height of the debris in the area inspected. Approximately 30% of the lower plenum region was inspected during the first camera inspection in February 1985.

A large quantity of debris of nonuniform size and appearance was seen in the regions surveyed. Little debris was seen near the Y-axis (see Figure A-1), while large quantities of debris were observed at the other locations. The debris appears to have accumulated to a depth of 30 to

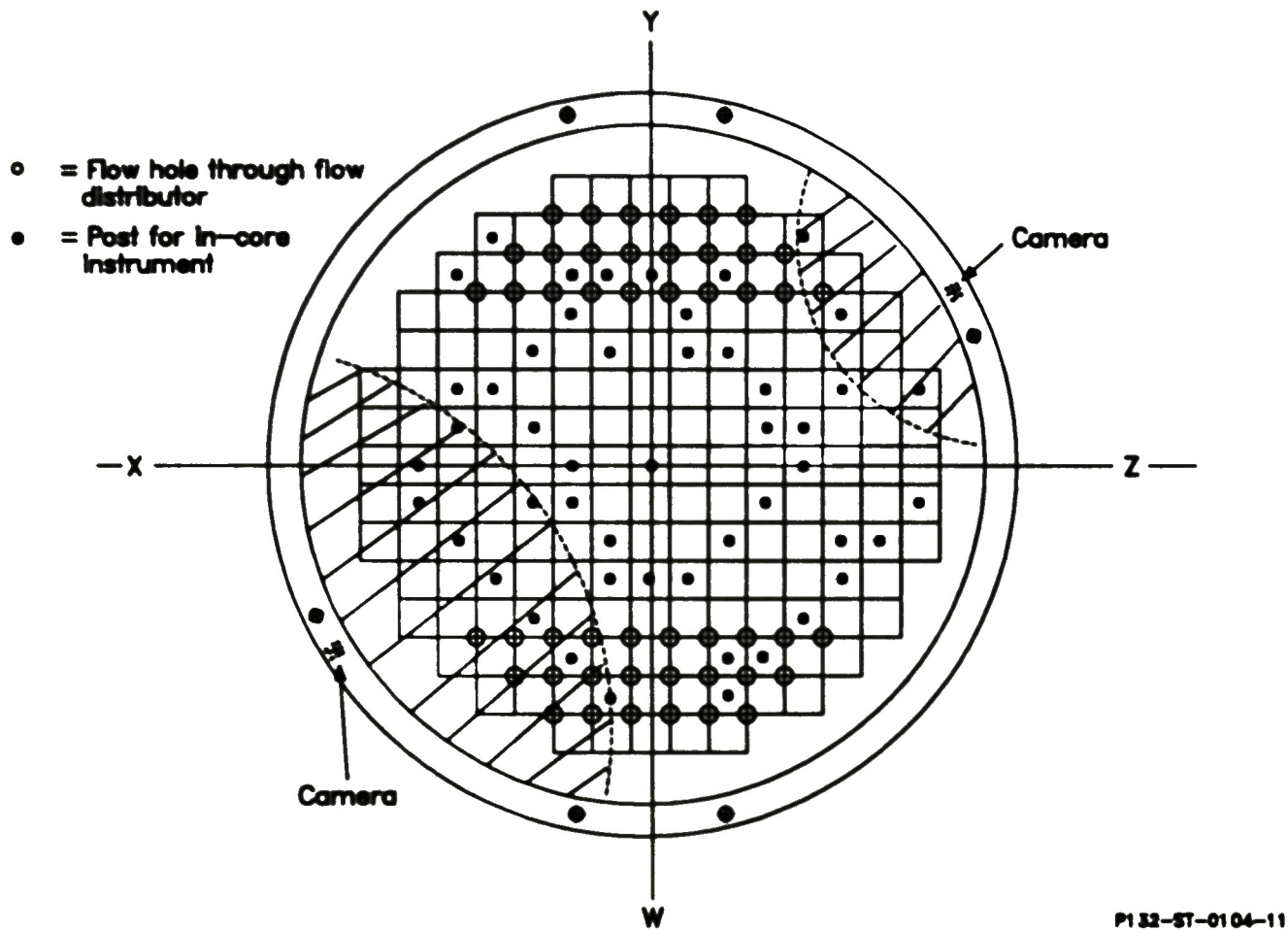

Figure A-1. Illustration of camera inspection regions of the TMI-2 lower plenum.

40 in. above the bottom invert of the head, and the shape of the debris pile seems to be higher at the edges than at the middle. By extrapolation from what was seen, it is estimated[A-1] that there may be from 10 to 20 tons of debris resting on the bottom head. The debris appears to be segregated radially, with the looser finer material near the center and the bigger chunks and agglomerations towards the edges. Debris chunks of consolidated material up to a few inches across or larger were observed, as well as what appears to be a mixture of loose material with particle sizes like sand to small gravel mixed together.

Specific details of debris and lower plenum structural characteristics, taken from still frames of the video tape, can be seen in Figures A-2 and A-3. Figure A-2 shows what appears to be frozen globular debris suspended from a hole in the flow distributor plate. The debris extends to about half the diameter of the flow hole (which is 6 in. in diameter) and is probably agglomerated once-molten material. The flow distributor plate itself showed no structural damage in any of the areas accessible for video inspection. Near one of the 6-in. flow holes, the characters "1A" had been stamped in the metal and were clearly visible. Figure A-3 shows a view of the debris bed in the region of the Inconel penetration nozzle and stainless steel guide tube junction. Although the Inconel penetration nozzle is shown to be intact above the surface of what appears to be a rather densely packed debris bed, this may not be the case below the debris surface. Following the video inspection, an attempt was made to penetrate the bottom-entry instrument tubes, which is summarized next.

Wire Probing of the Instrument Penetration Tubes

On March 21 and 22, 1985, a series of wire probings of the bottom-entry instrument penetration tubes (see Figures A-4, A-5, and A-6) using 60-mil, or 0.06-in.-dia wire was attempted to determine which tube locations might be used for later insertion of an ion chamber for gamma scanning of the lower plenum. The original intent was to probe 12 locations and to select six of these locations for gamma profiling.

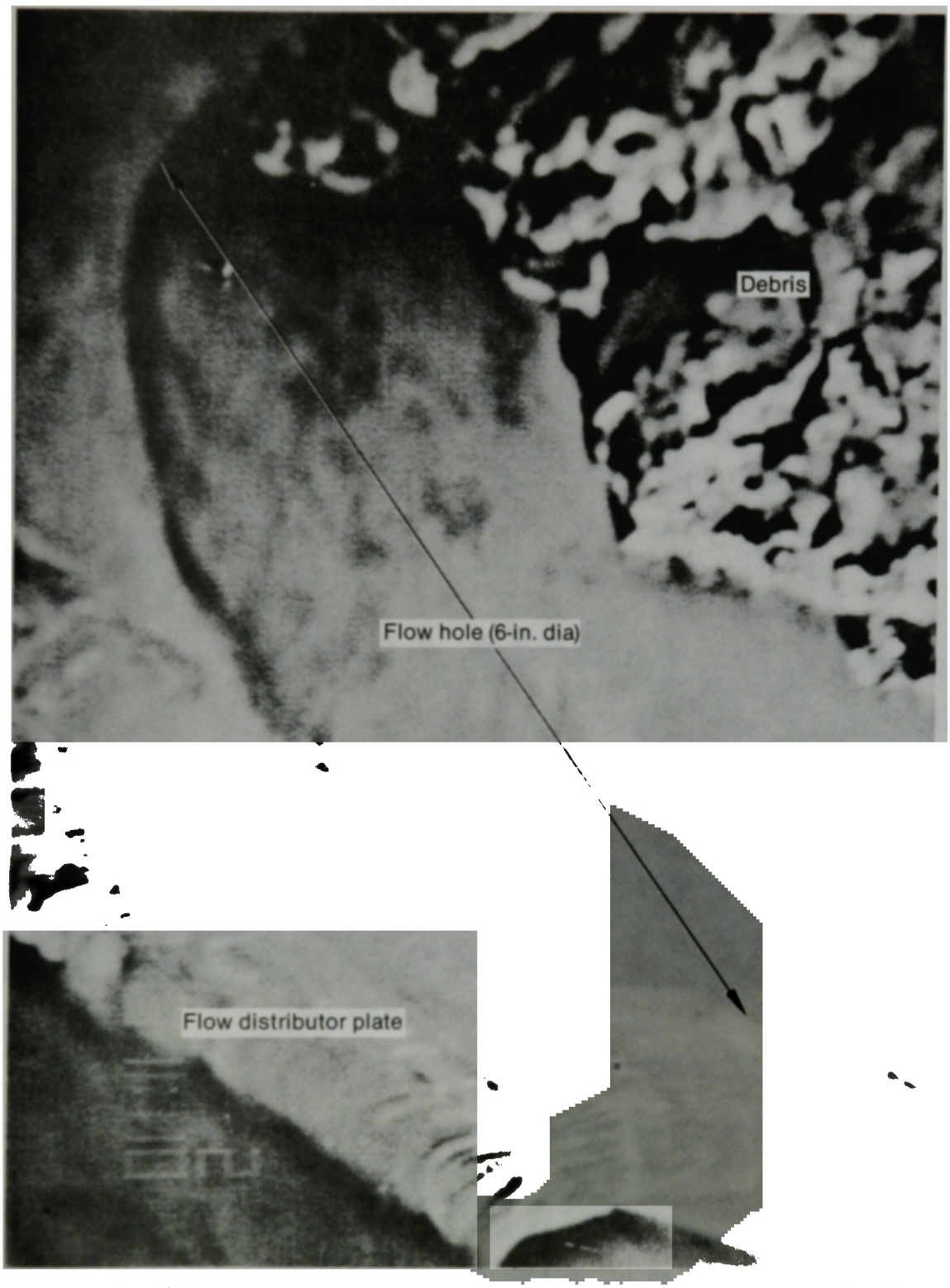

figure A-2. Illustration of once-molten TMI-2 core debris particle frozen within the flow hole of a flow distributor plate.

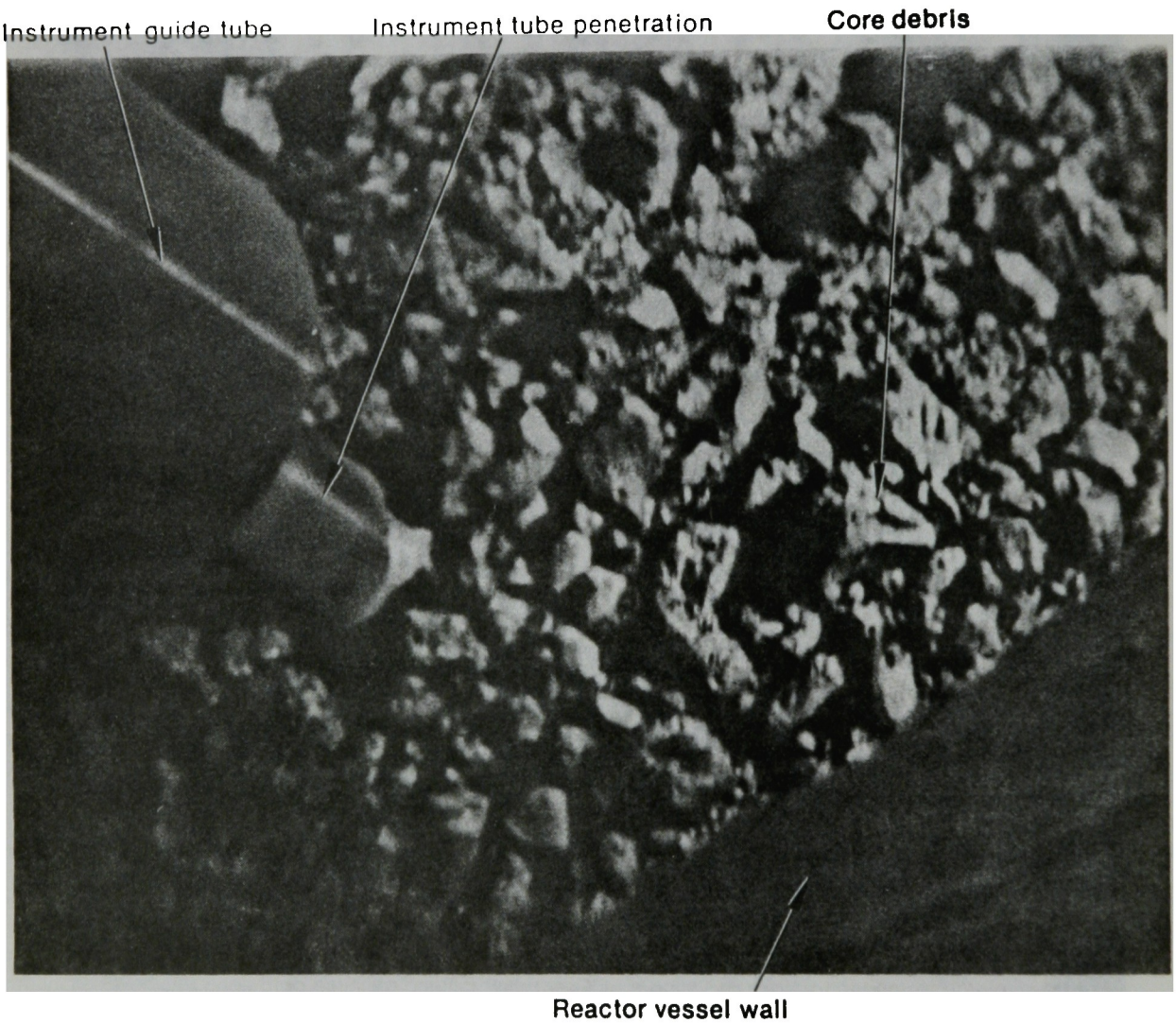

Figure A-3. Illustration of undamaged guide flange attached to flow distributor plate, indicating TMI-2 core debris pileup to within 4 in. of flow hole.

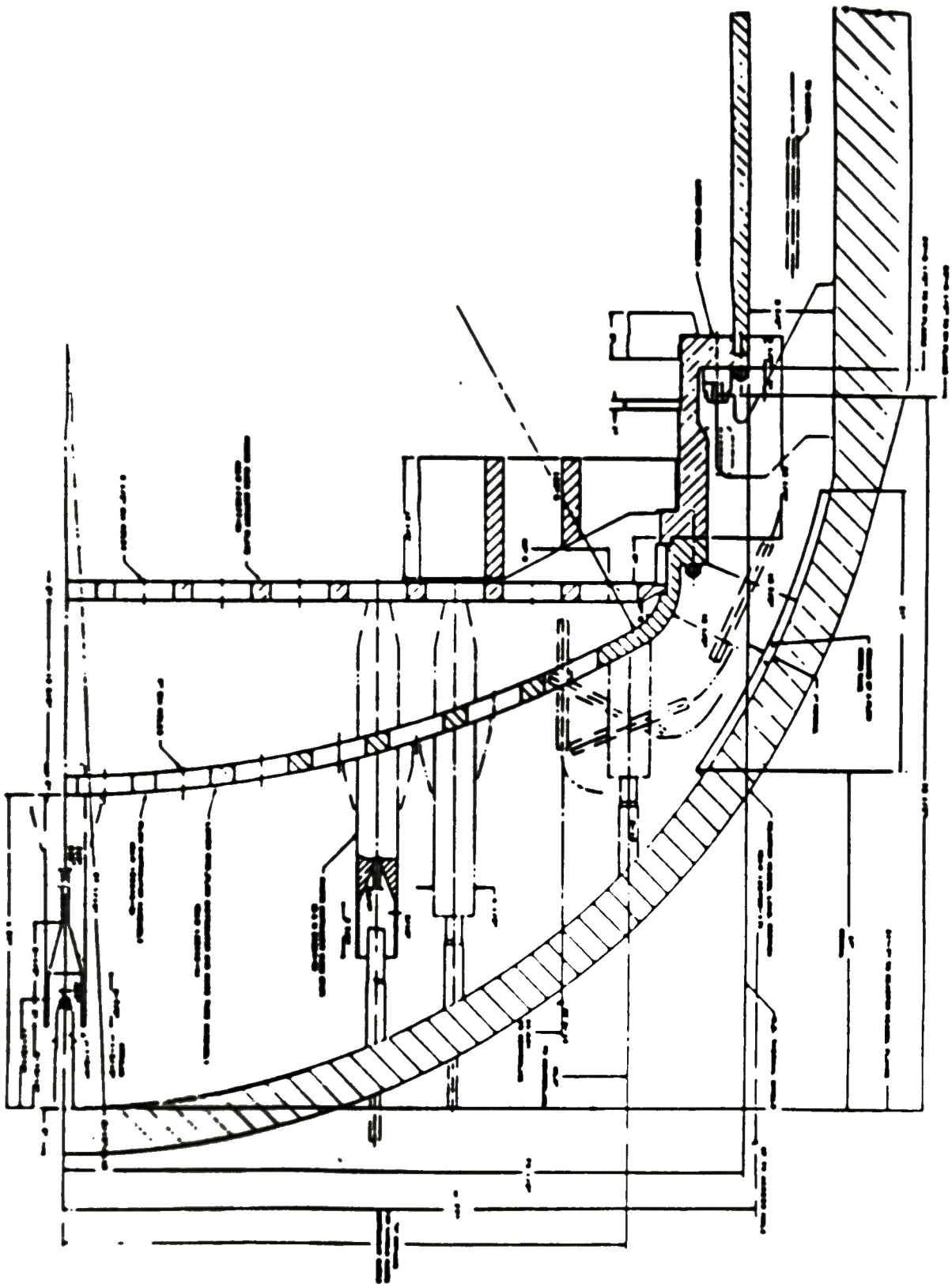

Figure A-4. Illustration of TMI-2 lower plenum region.

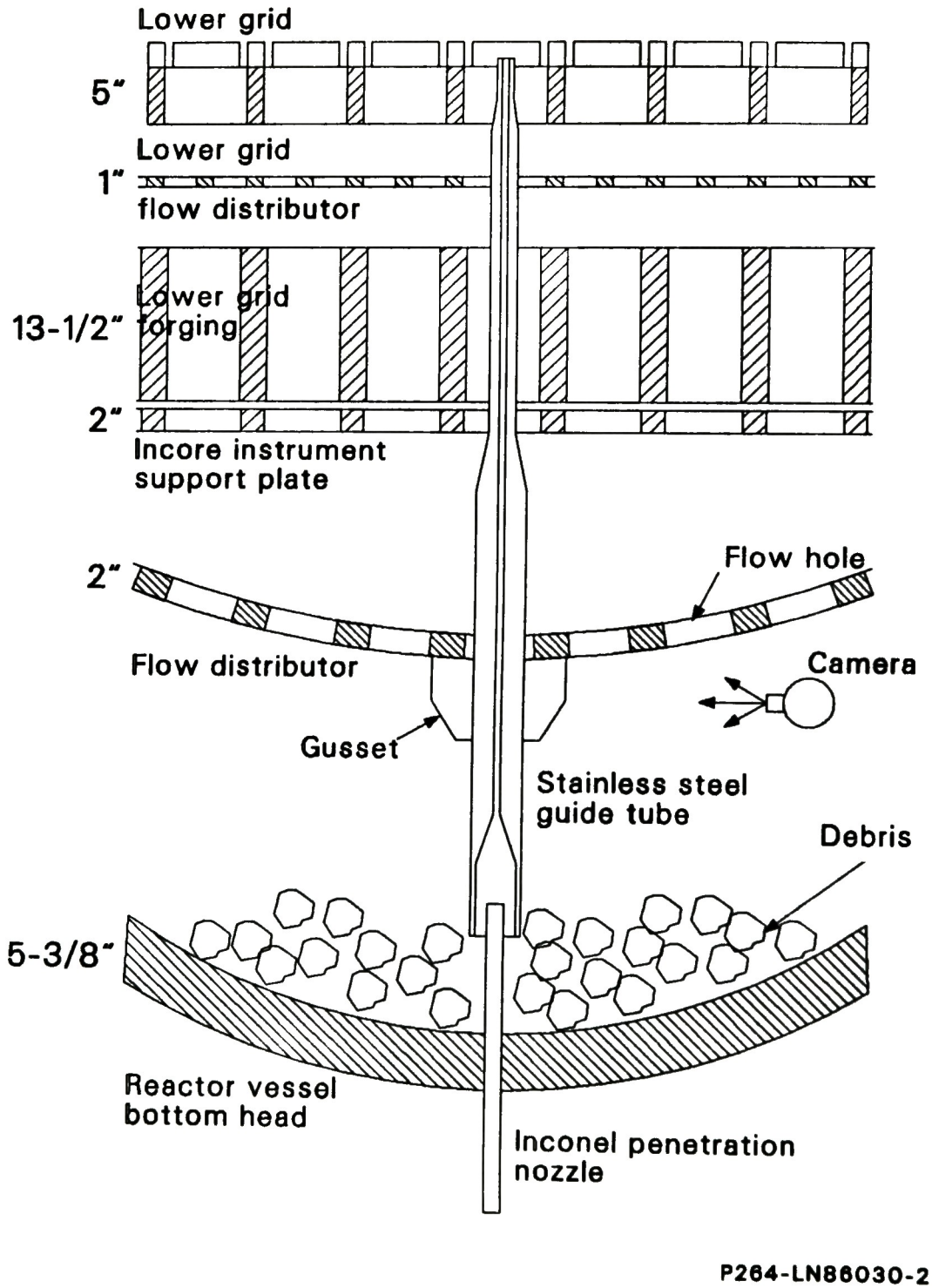

Figure A-5. Illustration of TMI-2 lower plenum region showing bottom-entry instrument penetration nozzle and guide tube.

Inconel Penetration Nozzle

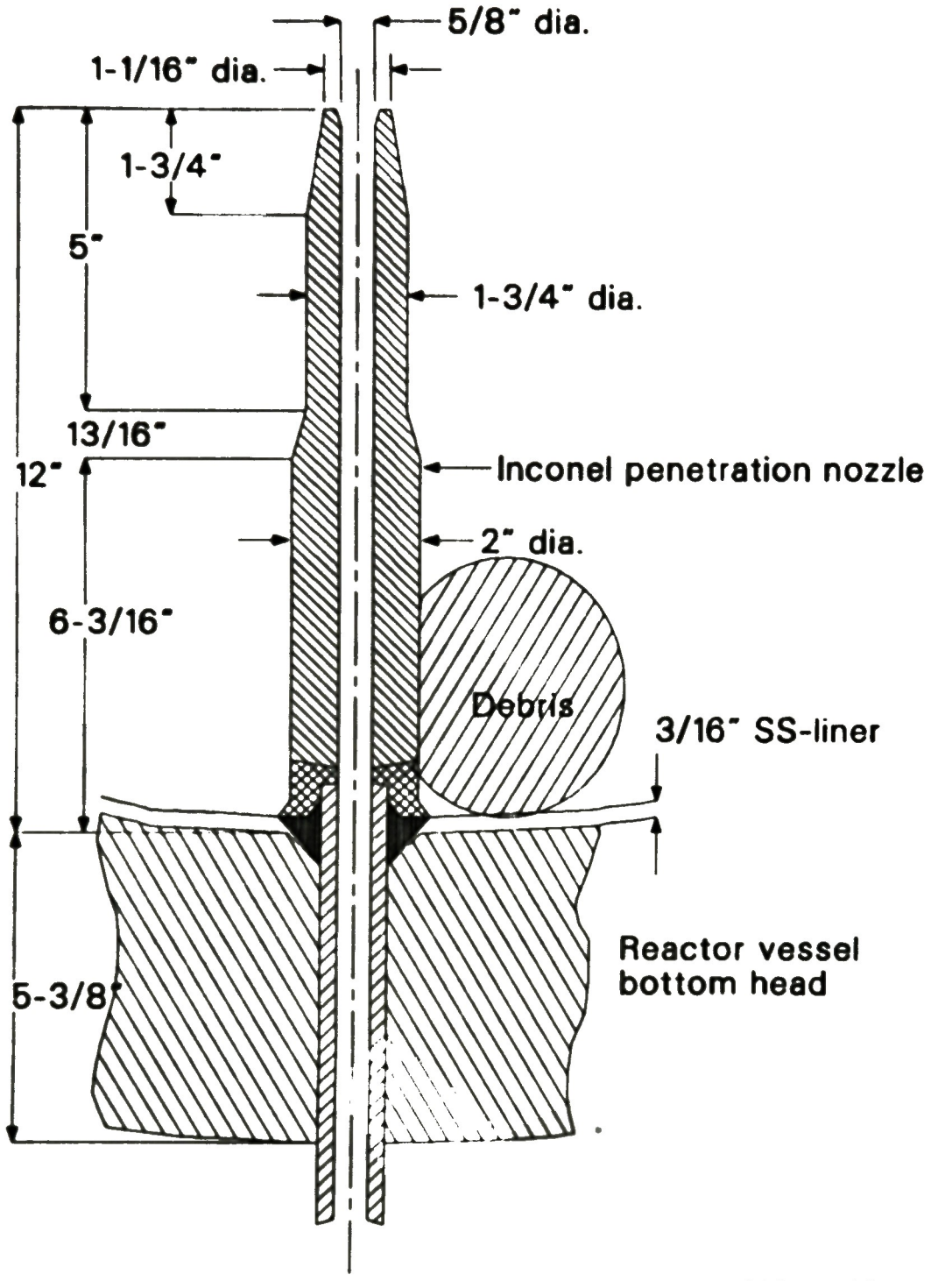

Figure A-6. Illustration of TMI-2 bottom-entry instrument penetration nozzle.

However, as shown in Table A-1, 17 locations were probed and 16 were found to be blocked at points outside the reactor vessel. The one location (L-11) which had access to the reactor vessel was subsequently gamma profiled. Although the wire probe penetrated more than 3 m (9 ft) above the reference plane at the bottom of the vessel, the ion chamber inserted later only penetrated 19 cm (≈7.4 inches), due to a slightly larger diameter. Since the penetration tube inside diameter (ID) is ~1.59 cm (0.625 in.), the implication of such wire probing is that a large portion of the penetration tubes are either filled with relatively fine debris or damaged by debris thermal attack of the tube walls.

Gamma Scanning of Lower Plenum

Following the wire probing effort, the single open penetration tube (L-11) was subjected to gamma scanning[A-5,A-6] via insertion of a thin-tube ion chamber. The purpose of such gamma probing was to quantify the amount and location of fuel debris within the lower plenum. Figure A-7 is a cross-section of the in-core instrument assembly inside its guide pipe, showing the central calibration tube into which the ion chamber was inserted. Figure A-8 shows the access path from the seal table in the containment building through the stainless steel guide tube, down to the containment basement, and upwards into the bottom of the reactor vessel.

The analysis was performed by comparing the measured gamma scan with calculated profiles, in an attempt to characterize the debris bed in terms of density and composition and retention of fission products. The detector had an outside diameter (OD) of 0.072 in. and a sensitive length of 1.67 in. The ion-chamber/detector cable was inserted into the calibration tube at the seal table in the reactor containment building (see Figure A-8) and manually advanced 108 ft into the calibration tube to a point 15.3 in. below the RV outer surface. Subsequent insertion of the chamber was via a positioning device that allowed advancing the chamber in 1-in. steps. At each step, the chamber signal was read via a digital electrometer and recorded. The gamma-scanning data are presented in Table A-2 and shown graphically in Figure A-9. Measured dose rates ranged from 23 R/h outside

TABLE A-1. TMI-2 BOTTOM-ENTRY INSTRUMENT TUBE PROBING RESULTS

1985 Date	Detection	Position	Probe Stop (ft)[a]	Thermocouple Pinch Point (ft)[b]	Comments
3/21	1	N-8	- 9.9[c]	4.0	Hard stop
3/22	4	F-8	- 6.7[c]	1.2	Hard stop
3/22	6	F-7	-10.8[c]	1.2	Hard stop
3/21	7	E-7	-18.9[c]	0.9	Gritty, hard stop
3/22	11	K-5	-15.4[d]	13.7	Sandy stop
3/22	13	M-8	- 0.5 (in.)[e]	9.9	Hard stop
3/22	16	M-9	- 4.2[e]	0.7	Sandy, hard stop
3/21	18	L-11	+ 9.6[e]	12.6	Hard stop
3/22	20	K-12	-15.0[d]	--	Hard stop
3/21	24	F-12	-18.0[e]	13.6	Gritty, hard stop
3/22	26	E-11	-36.2[d]	0	Water displaced
3/21	33	D-5	-25.5[d]	11.6	Solid stop
3/22	34	E-4	- 7.9[d]	--	Hard stop
3/22	36	G-2	- 0.9[d]	10.6	Hard stop, moisture on probe
3/22	41	N-4	--	12.0	Not probed, water seeped out after uncapping tube
3/22	49	M-14	-15.0[d]	5.5	Hard stop, moisture on probe
3/22	51	D-14	-39.8[d]	14.4	Hard stop, water in tube
3/22	52	C-13	- 7.9[d]	10.6	Hard stop

a. The reported values in feet refer to the height above the reactor vessel base elevation (290' 5-1/4").

b. From GEND-INF-031, Vol. II.

c. Measured with tape measure.

d. Distance estimated from number of loops in cable.

e. Rough estimate.

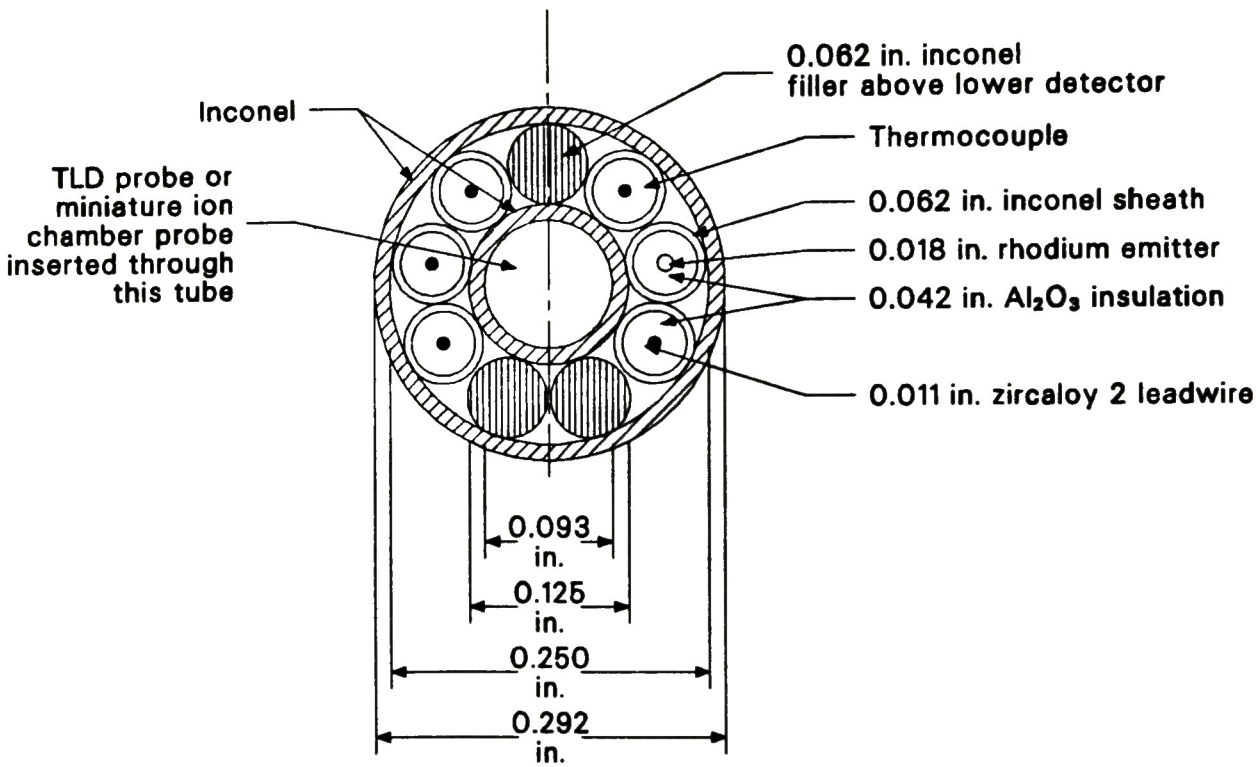

(Assembly includes seven neutron-sensitive detectors, one background detector, and one thermocouple.)

P264-LN86030-1

Figure A-7 Illustration of TMI-2 bottom-entry detector cross section; center hole serves as an access port for insertion of miniature ion chamber for gamma survey of lower plenum.

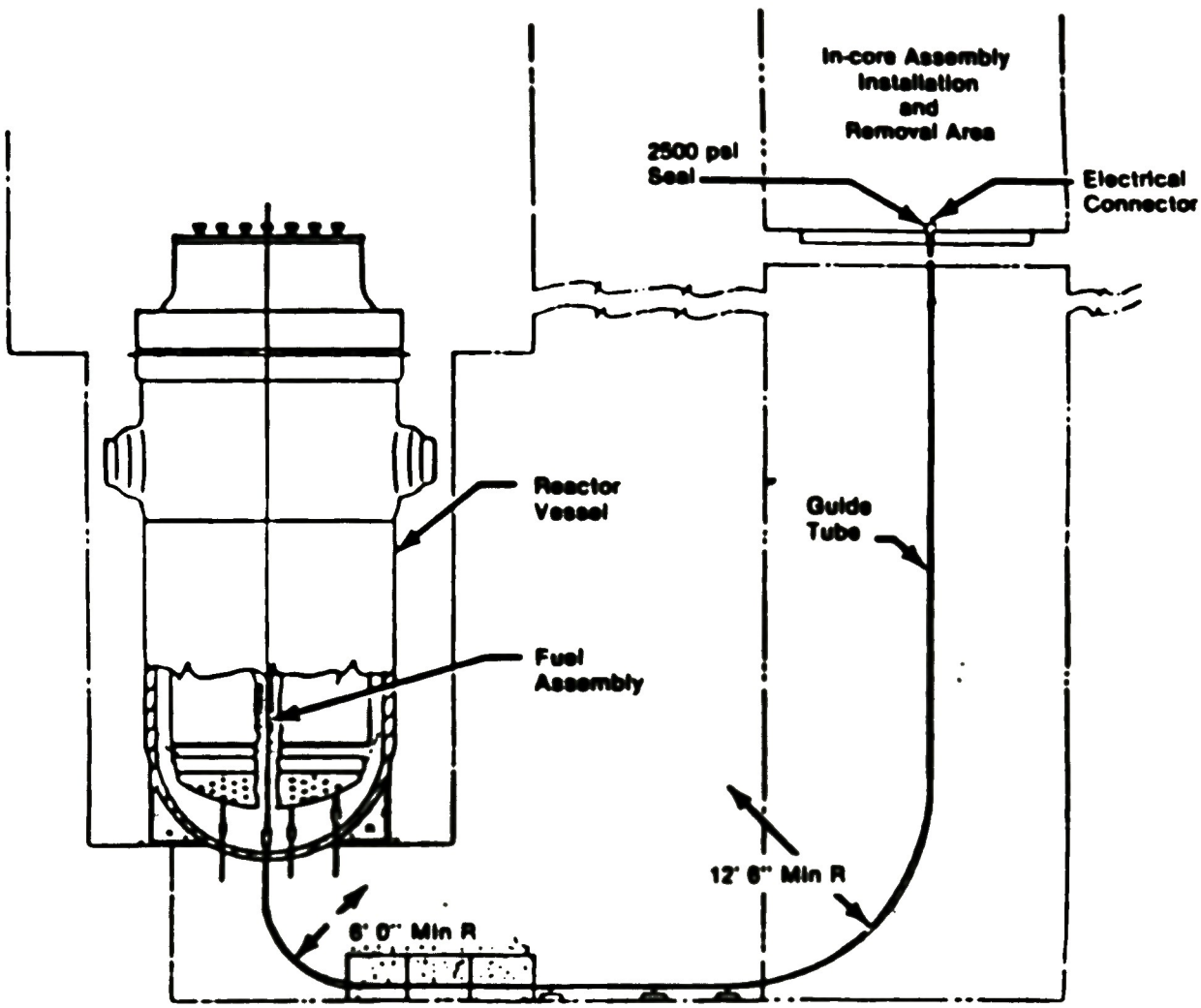

Figure A-8. Guide tube layout for TMI-2 bottom-entry instrument insertion and removal.

TABLE A-2. GAMMA SCANNING OF IN-CORE DETECTORS GAMMA PROFILE AT GRID POSITION L-11 (#18)

Detector Elevation Relative to RV Inner Surface at L-11 (cm)	Measured Dose Rate in Center Calibration Tube[a] (R/hr)	Location of Detector Centerline
-15.5	4.6	Vessel shell
-12.9	4.6	Vessel shell
-10.4	3.4	Vessel shell
- 7.9	1.8	Vessel shell
- 5.3	1.2	Vessel shell
- 2.8	2.2	Vessel shell
- 0.3	4.6	Vessel shell
0.0	[b]	RV inner surface
2.3	11.0	Debris bed
4.8	24.2	Debris bed
7.4	41.4	Debris bed
9.9	66.6	Debris bed
12.4	86.2	Debris bed
15.0	96.0	Debris bed
17.5	99.4	Debris bed
18.8	100.0	Debris bed

a. Obtained by use of a gamma sensitivity of 17.41×10^{-13} amp/R/h for the ion-chamber.

b. Not measured.

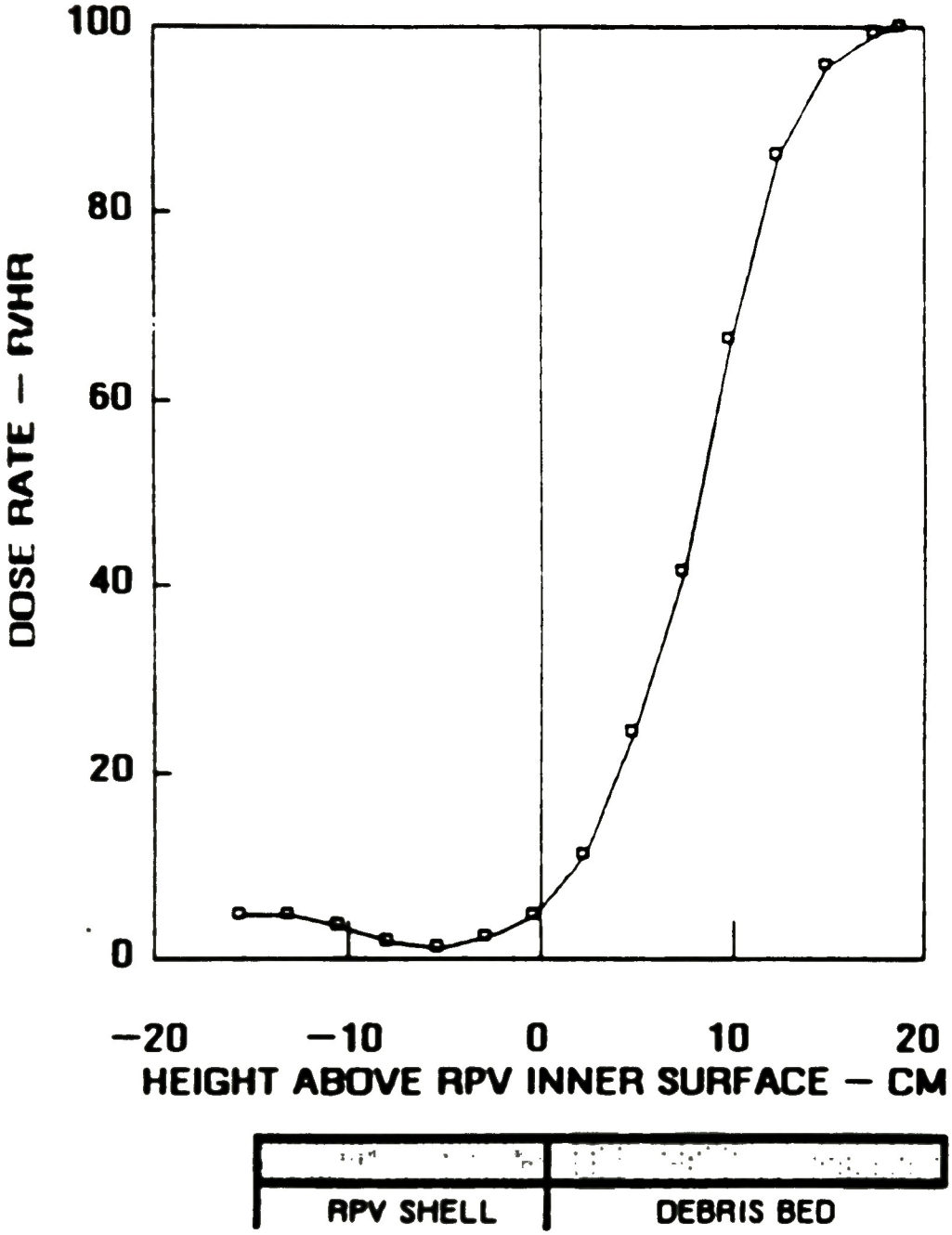

Figure A-9. Gamma-scanning results at TMI-2 in-core detector location L-11.

the RV to a maximum reading of 100 R/h at the location where the detector was blocked inside the vessel [~18.8 cm (7.4 in.) above the inner surface of the reactor vessel].

The fact that the activity increases with increased height suggests the existence of a non-fuel layer at the very bottom of the lower plenum. This observation, in combination with the presence of 2750 kg of Ag-In-Cd (80 wt.% silver, 15 wt.% indium, 5 wt.% cadmium) in the as-built TMI-2 core and the relatively low-melting point [1072 K (1470°F)] of the control rod alloy, prompted further investigation. The dose rate profile calculations, in conjunction with the 2750-kg inventory of control rod material in the as-built core, indicated a non-fuel debris layer having a height of approximately 9 in. at the center position (H-8), which corresponds to a layer height of ~3 inches at the L-11 position. It is thus possible that a non-fuel layer exists at the very bottom of the TMI-2 lower plenum, which represents resolidified Ag-In-Cd alloy with an overlayer of fuel debris, as depicted in Figure A-10.

Based on gamma-scanning measurements, the following lower plenum debris characterization was made:

- The specific activities of the debris in the lower plenum appear to be significantly lower than the measured values of the debris grab samples previously taken from the upper TMI-2 core region. This suggests that the debris in the lower plenum may have been subjected to temperatures in excess of 2000 K, so as to boil off medium-volatility fission products.

- The debris in the lower plenum may also contain a high percentage of non-fuel metallic material, which includes metallic elements such as iron, nickel, and/or silver.

- The gamma-scanning study suggests that a non-fuel layer exists at the very bottom of the RV lower head. Calculations indicate the reference layer has a height of approximately 9 in. at the center

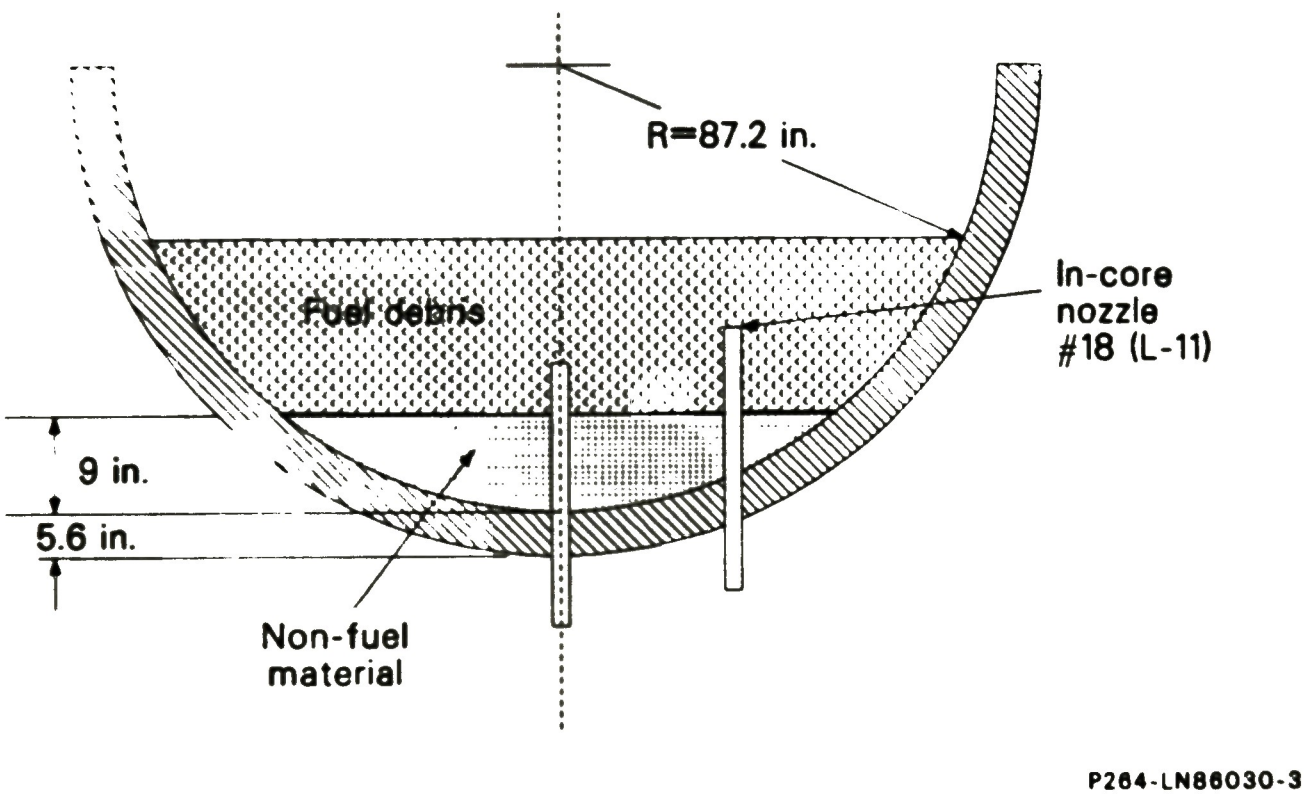

Figure A-10. Illustration of lower plenum debris configuration based on gamma-scan probe through TMI-2 bottom-entry penetration nozzle at L-11 location.

(H-8) and an outer radius of ~39 in. The calculated volume of the layer is estimated to 0.34 m^3. It is possible that this non-fuel layer represents resolidified absorber material (Ag-In-Cd) from the control rods.

Besides the gamma-scanning effort, a hydraulic disturbance of the debris bed was attempted to assess if the material could be characterized as loose rubble. This effort is briefly summarized next.

Hydraulic Disturbance of Debris Bed

On July 23, 1985 a hydraulic spray nozzle was inserted into the bottom head region of the TMI-2 reactor vessel. The nozzle tip was placed at a location more or less below hole number 11 in the CSA flange. This location was chosen because the debris there appeared to be large chunks. The purpose was to see if the debris was fused together or movable and, if movable, to see what was beneath the surface when the loose material was moved.

Borated water was delivered to the nozzle tool for 2 min, at a pressure of 2500 psi for the first minute and 5000 psi for the second minute. Visibility deteriorated to almost zero as soon as the jet was activated. The finer debris material became suspended but settled quickly; water clarity was reestablished 30 min after the disturbance. A crater in the debris was visible after the flush.

Based on this study, a good fraction of the debris in the lower plenum appears to be in a loose rubble configuration and easily movable. Since the debris was found to be loose, a subsequent study involved debris sample retrieval, as discussed next.

Debris Sample Retrieval

During late July 1985, a successful attempt was made to retrieve loose debris samples from the lower plenum region. Using a long manipulating

tool with a finger gripper at the end, samples were obtained from two azimuthal locations (see Figure A-1), one near the X-axis and one near the W-axis. The samples were obtained individually and were placed in two 3-in.-ID buckets. Six samples, ranging from an estimated 0.25 to 1.25 in. in size, were retrieved from the W-axis (Set No. 1). Approximately 5 or 6 samples were obtained from near the X-axis (Set No. 2), one debris chunk being about 2.75 in. in diameter. Limited visual examination indicates that the samples vary in appearance and size. Future detailed analyses of these samples will provide information on the material content, mechanical properties, and fuel and fission product content.

REFERENCES

A-1. Technical Planning Department, April 1985, Determination of Fuel Distribution in TMI-2 Based on Axial Neutron Flux Profile, TPO/TMI-165, Rev. 0, GPU Nuclear Corporation.

A-2. R. Gold et al., Solid-State Recorder Neutron Dosimetry in the Three Mile Island Unit-2 Reactor Cavity, GEND-INF-059, May 1985.

A-3. V. R. Fricke, Reactor Lower Head Video Inspection, TMI-2 Technical Planning Bulletin, TPB-85-6, February 26, 1985.

A-4. D. G. Keefer, "In-Core Instruments Tube Probing," EGG-Interoffice Correspondence, April 1, 1985.

A-5. R. Rainisch, Gamma Scanning of In-Core Detectors, TMI-2 Technical Planning Bulletin, April 23, 1985.

A-6. R. Rainisch, Analysis of Gamma Scanning of In-Core Detector No. 18 L-11 in Lower Reactor Vessel Head, GPU Nuclear Report TPO/TMI-175, June 1985.

A-7. V. R. Fricke, Hydraulic Disturbance of the Debris in the Bottom Head of the TMI-2 Vessel, TMI-2 Technical Planning Bulletin, TPB-85-20, July 26, 1985.

A-8. G. Worku, Core Debris Sample Retrieval from the Lower Head Region, TMI-2 Technical Planning Bulletin, TPB-85-21, July 29. 1985.

APPENDIX B

ESTIMATE OF DRAINAGE VELOCITY AND FRICTION FACTOR

APPENDIX B

ESTIMATE OF DRAINAGE VELOCITY AND FRICTION FACTOR

Figure B-1 illustrates the equivalent flow-channel mockup for viscous melt drainage in an open channel. As indicated, the drainage characteristics can be assessed from a force balance, where the effects of gravity flow are counteracted by wall frictional forces; i.e.:

$$m \frac{dV}{dt} = F_g - F_f \qquad (B\text{-}1)$$

where m is the slug mass and dV/dt is acceleration. The slug mass, gravitational force, and frictional force can be expressed as follows:

$$m = (\rho AH)$$
$$F_g = (\rho AH)g$$
$$F_f = 4f\ (H/D_e)\ \rho A\ (V^2/2)$$

where f is frictional factor, A is the cross-sectional flow area, H is height, D_e is equivalent diameter, ρ is density, g is gravity constant, and V is velocity. Eliminating common terms, the acceleration can be expressed as:

$$\frac{dV}{dt} = g - \frac{2f}{D_e} V^2 \qquad (B\text{-}2)$$

For smooth walls, the Blasius correlation can be used to assess the friction factor f:

$$f = 0.316/Re^{.25} \quad \text{where} \quad Re = \rho V D_e/\mu \qquad (B\text{-}3)$$

Noting that the friction factor is a relatively weak function of velocity, a constant value of f is assumed; thus, the momentum equation can be directly integrated as follows:

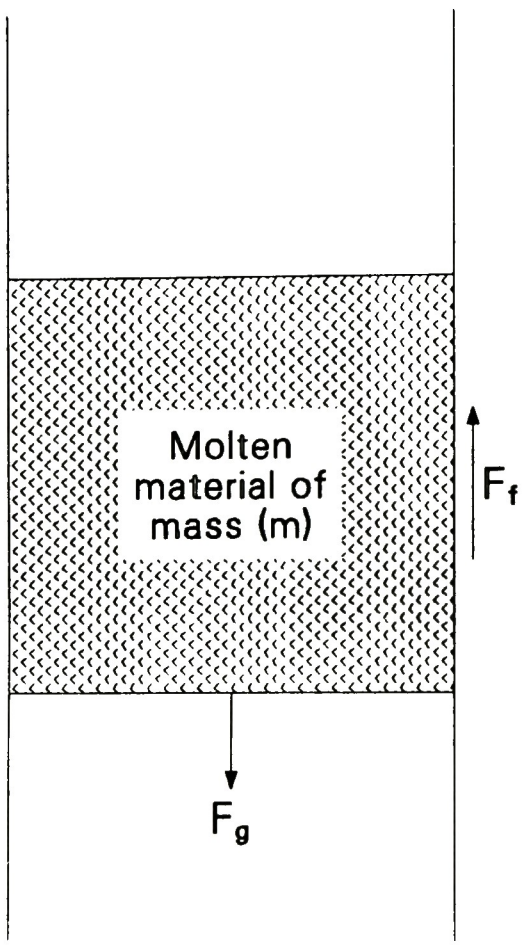

F_g = force of gravity

F_f = friction force

$$m \frac{dV}{dt} = F_g + \Sigma F_f$$

LP264-LN86030-8

Figure B-1. Illustration of viscous flow in an open channel.

$$\frac{dV}{dt} = g - BV^2 \qquad \text{where } B = 2f/D_e$$

$$\frac{1}{B}\frac{dV}{dt} = A^2 - V^2 \qquad \text{where } A^2 = g/B;\ A = (g/B)^{0.5}$$

$$\int_0^V \frac{dV}{A^2 - V^2} = \int_0^t B\,dt$$

$$\frac{1}{2A} \ln \left(\frac{A + V}{A - V}\right) = Bt$$

$$\left(\frac{A + V}{A - V}\right) = e^{2ABt}$$

Solving for the drainage velocity as a function of time, we obtain

$$V(t) = A \left[\frac{\exp(2ABt) - 1}{\exp(2ABt) + 1}\right]$$

The solution to the above equation, summarized in Table B-1, involves iteration between f and V, where an average velocity, V, is first assumed to estimate the friction factor, f, which is then inserted into the above equation to estimate the drainage velocity. If the assumed value of V for estimation of f closely approximates the predicted value of V, then the solution is obtained. As indicated, the terminal velocity of 183 cm/s is reached in ~1 s. Since the assumed average velocity for calculation of the average friction factor was 100 cm/s, the solution is applicable (i.e., the average velocity would be about half the terminal velocity).

TABLE B-1. ESTIMATE OF DRAINAGE CHARACTERISTICS OF MOLTEN MATERIAL DRAINAGE THROUGH THE TMI-2 BOTTOM-ENTRY INSTRUMENT NOZZLE

Governing Equation:

$$V(t) = A\left[\frac{\exp(2ABt) - 1}{\exp(2ABt) + 1}\right]$$

$A = g/B$
$B = 2f/D_e$

Parameter Values (Based on TMI-2 Instrument Nozzle Dimensions):

g = gravitation constant = 32.2 ft/s^2 = 980 cm/s^2

D_e = flow diameter = 0.625 in. = 1.59 cm

Estimate of f

$f = 0.316/Re^{.25}$ (Blasius Relation)

$$Re = \frac{D_e V \rho}{\mu}$$

$\mu = 4(10^{-2})$ g/cm-s (molten UO_2

$V \sim 100$ cm/s (assumed) = 3.28 ft/s

$\rho = 9$ g/cm^3 (molten UO_2

$Re = 1.59\ (100)(9)/0.04 = 35{,}775$

$Re^{0.25} = 12.75$

$f = 0.023$

Values of A and B

$B = 2f/D_e = 0.029$ 1/cm
$A = (g/B)^{0.5} = (980/0.029)^{0.5} = 183$ cm/s

Initial and Terminal Velocity

$t = 0.0$ $V = 0.0$ cm/s (initial)
$t =$ $V = 183$ cm/s (terminal)

Time to Reach Terminal Velocity

t(s)	V (cm/s)
0.01	10.4
0.1	88.9
1.0	183.0